FLEXIBLE TRANSPARENT CONDUCTING ELECTRODES BASED ON SILVER NANOWIRE, GRAPHENE, AND TWO-DIMENSIONAL TRANSITION METAL DICHALCOGENIDE

A Thesis Submitted to
Graduate School of Engineering and Sciences of
İzmir Institute of Technology
in Partial Fulfillment of the Requirements for the Degree of

MASTER OF SCIENCE

in Photonics Science and Engineering

by
Necip Ayhan TERTEMİZ

December 2020
İZMİR

ACKNOWLEDGMENTS

I am grateful because I managed to complete my master of science within the given time by my respectful advisor Assoc. Prof. Dr. Sinan BALCI and Fadime Mert BALCI. I would like to thank committee members of my thesis Assoc. Prof. Dr. Engin KARABUDAK and Assoc. Prof. Dr. İlknur TUNÇ for their participation and constructive comments about my thesis.

ABSTRACT

FLEXIBLE TRANSPARENT CONDUCTING ELECTRODES BASED ON SILVER NANOWIRE, GRAPHENE, AND TWO-DIMENSIONAL TRANSITION METAL DICHALGOGENIDE

In recent years, transparent conductive electrodes have attracted great interests owing to their critical applications in various optoelectronic devices, such as light emitting diodes, solar cells, liquid crystal displays, optical modulators, and touch screens. In this thesis, graphene-silver nanowires-transition metal dichalcogenide based hybrid transparent and conductive electrodes have been fabricated. In order to reach this goal; (1) single layer graphene on copper foil has been synthesized in large area in a CVD furnace, (2) ultrathin and very long silver nanowires have been synthesized by using wet chemistry methods, (3) MoS_2 and WS_2 single layer flakes and multilayer thin films have been synthesized in a CVD furnace, (4) electrodes of graphene, silver nanowires, and transition metal dichalcogenides have been fabricated on rigid and flexible substrates.

ÖZET

GÜMÜŞ NANOTEL, GRAFEN VE İKİ-BOYUTLU GEÇİŞ METAL DİKALKOJENİD TEMELLİ ESNEK ŞEFFAF İLETKEN ELEKTRODLAR

Son yıllarda, şeffaf iletken elektrodlar, ışık yayan diyotlar, güneş hücreleri, sıvı Kristal ekranlar, optic modülatörler ve dokunmatik ekranlar gibi çeşitli optoelektronik cihazlardaki kritik uygulamaları nedeniyle büyük ilgi gördü. Bu tezde grafen-gümüş nanoteller-geçiş metal dikalkojenit esaslı hibrit şeffaf ve iletken elektrotlar üretilmiştir. Bu hedefe ulaşmak için; (1) Bakır folyo üzerine tek katmanlı grafen bir CVD fırınında geniş bir alanda sentezlenmiş, (2) ultra ince ve çok uzun gümüş nanoteller ıslak kimya yöntemleri kullanılarak sentezlenmiştir, (3) MoS2 ve WS2 tek katmanlı pullar ve çok katmanlı ince filmler bir CVD fırınında sentezlenmiştir, (4) grafen elektrotları, gümüş nanoteller ve geçiş metali dikalkojenidleri sert ve esnek substratlar üzerinde imal edilmiştir.

To my dear family

TABLE OF CONTENTS

LIST OF FIGURES……...vii

CHAPTER 1. INTRODUCTION 1

1.1. Graphene 1

1.1.1. Raman Spectroscopy of Graphene 3

1.1.2. Electronic Properties of Graphene.....6

1.1.3. Optical Properties of Graphene 8

1.2. Silver Nanowires.....9

1.2.1. Properties and Performance of the Silver Nanowire 11

1.3. Transition Metal Dichalcogenides 12

1.3.1. Crystal Structure of TMDCs.....12

1.3.2. Electronic Band Structure of TMDCs 13

1.3.3. Characterization Methods of TMDCs 15

1.3.4. Molybdenum Disulfide.....16

1.3.5. Tungsten Disulfide 18

CHAPTER 2. EXPERIMENTAL METHODS AND RESULTS 21

2.1. Synthesis and Transfer of Graphene 21

2.2. Synthesis and Transfer of TMDC 22

2.3. Synthesis and Transfer of Molybdenum Disulfide 22

2.4. Synthesis and Transfer of Tungsten Disulfide.....23

2.5. Synthesis and Purification of Silver Nanowire.....23

2.6. Optical Measurements 24

2.7. Electrical Measurements.....30

CHAPTER 3. RESULTS AND DISCUSSIONS 36

CHAPTER 4. CONCLUSION 38

REFERENCES 39

LIST OF FIGURES

Figure **Page**

Figure 1. The basic unit of carbon nanotube, buckyball, and graphite is graphene having hexagonal latticed carbon atoms 1
Figure 2. Raman spectra of graphene and graphite. The G and 2D bands reflecting the structural properties of the samples are clearly visible in the spectra 4
Figure 3. Raman spectra of the defective Graphene.(Beams, Gustavo Cançado, and Novotny 2015).....5
Figure 4. Honeycomb lattice of graphene and its Brillouin zone.....6
Figure 5. 2D and 3D band structure of graphene.(J. Wang et al. 2017).....7
Figure 6. Intraband and interband electronic transitions in graphene.(Yakar 2020).....8
Figure 7. (a) Low-magnification FE-SEM image of the synthesized AgNWs; and (b) High-magnification FE-SEM image of the synthesized AgNWs. (Y. Li et al. 2019).....10
Figure 8. Crystal structure of TMDC.(Q. H. Wang et al. 2012) 13
Figure 9. Electronic band structures of MoS_2 and WS_2 ; a)MoS_2, b)WS_2. (Kuc and Heine.2015) 14
Figure 10. AFM characterization of MoS_2; a) AFM image of a grown MoS_2 monolayer film, b) height profile of the MoS_2 thin film. (Senthilkumar et al. 2014).....17
Figure 11. Raman and PL spectra of MoS_2; (a) Raman spectra of different layer number, (b) PL spectrum of monolayer MoS_2. (Splendiani et al. 2010; Ganorkar et al., n.d.) 17
Figure 12. (a) Raman spectra measurements; Raman shift of different layers of WS2, (b) The frequency of the Raman shift as a function of the layer number.(Qiao et al.2017) 19
Figure 13. PL spectra of bulk, one-layer, two-layer, and three-layer tungsten disulfide 20
Figure 14. Optical microscopy image, (b) AFM image, and (c) Height profile of WS_2.(Khairuzzaman 2016) 20

Figure **Page**

Figure 15. Optical microscopy image of Co catalyzed AgNWs on a glass substrate....24
Figure 16. Transmittance of the Co catalyzed electrode containing Ag nanowires on a glass substrate.. 25
Figure 17. Optical microscopy image of Cr catalyzed AgNWs coated on a glass substrate....26
Figure 18. Transmittance of the Cr catalyzed electrode containing Ag nanowires on a glass substrate 26
Figure 19. Optical microscopy image of Mn catalyzed AgNWs on a glass substrate....27
Figure 20. Transmittance of the Mn catalyzed electrode containing Ag nanowires on a glass substrate 28
Figure 21. Transmittance of the Cu catalyzed electrode containing Ag nanowires, graphene and WS_2 on a glass substrate....29
Figure 22. Transmittance of the Cu catalyzed electrode containing Ag nanowires, graphene and MoS_2 on a glass substrate....29
Figure 23. Resistance change of transparent conducting thin films fabricated by using Co catalyzed AgNWs with annealing time 31
Figure 24. Resistance change of transparent conducting thin films fabricated by using Cr catalyzed AgNWs with annealing time 31
Figure 25. Resistance change of transparent conducting thin films fabricated by using Mn catalyzed AgNWs with annealing time....32
Figure 26. Resistance change of transparent conducting thin films fabricated by using Cu catalyzed AgNWs with annealing time 32
Figure 27. Bending effects on the resistance of the transparent conducting electrode fabricated by using Co catalyzed AgNWs....33
Figure 28. Bending effects on the resistance of the transparent conducting electrode fabricated by using Cr catalyzed AgNWs 34
Figure 29. Bending effects on the resistance of the transparent conducting electrode fabricated by using Cu catalyzed AgNWs....34
Figure 30. Bending effects on the resistance of the transparent conducting electrode fabricated by using Mn catalyzed AgNWs....35

CHAPTER 1

INTRODUCTION

1.1. Graphene

In 2004, graphene, for the first time, was shown experimentally as a new two-dimensional material and it became a rising star for many research areas due to its extraordinary mechanical, optical, and electrical properties. The first experiments were done by exfoliating the graphite with a scotch tape until achieving the one atom thickness.(K. S. Novoselov, A. K. Geim, S. V. Morozov, D. Jiang, Y. Zhang, S. V. Dubonos 2016) Graphene is a sp^2 hybridized new class of material and its name comes from a graphite because it is one atom thick graphite. Graphene has monolayer packed carbon atoms in a honeycomb lattice structure and it has two carbon atoms in a single unit cell. Unlike graphene, graphitic honeycomb latticed materials have also other dimensionalities like 0D fullerenes, 1D nanotubes or 3D graphite.

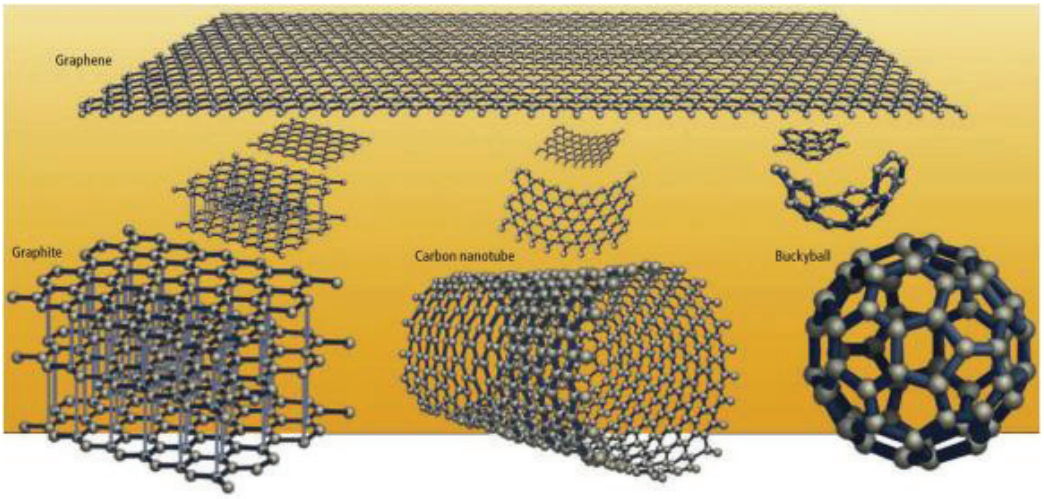

Figure 1. The basic unit of carbon nanotube, buckyball, and graphite is graphene having hexagonal latticed carbon atoms.(Source : J. Wang et al. 2017) The carbon atoms in all of them are sp^2 hybridized.

Each carbon compounds have unique individual electronic and mechanical properties. For example, while the electrical conductivity of fullerene is $10^{-10}\ S\ cm^{-1}$, electrical conductivity of carbon nanotubes is shape dependent.(Castro Neto et al. 2009) In the case of graphene, the electronic structure of the graphene is layer dependent and thus the electrical conductivity of graphene rapidly evolves with the increasing number of graphene layer. Monolayer and bilayer graphene have similar electronic spectra and they are zero-gap semiconductor or semi-metal. The electronic spectra of multilayer graphene change for three or more layers like appearing the several charge carriers, overlapping the conduction and valance bands.(Castro Neto et al. 2009) As a result of unique energy band structure of graphene, graphene has extraordinary electronic and optical properties. These properties lend the usage of graphene in many areas, such as field-effect transistors, memory devices, sensing platform, photovoltaic devices, flexible electronics, and also as an infrared camouflage material(Salihoglu et al. 2018) and a transparent electrode as well.(Huang et al. 2011) Most of the reported applications of graphene in various fields require changing the charge density and Fermi energy level of graphene by application of a gate voltage.

The number of electrons and holes per unit volume implies the charge density or charge carrier concentration. The optical and electronic properties of graphene are strongly influenced by the charge carrier density. The charge carrier density of graphene can be varied by using variety of techniques, for example, electrostatically(Lee et al. 2008), chemically(H. I. Wang et al. 2017) or by photo-induction(Kim et al. 2012). Changing the carrier concentration of graphene shifts the Fermi level of graphene and this shift determines doping level of graphene. There are two types of doping, negative (n) and positive (p). In the case of negative doping, the number of electrons is greater than the number of holes and the vice versa for positive doping.(Avouris 2010)

Until now, various synthesis techniques have been shown in the literature to synthesize single layer graphene. These techniques are exfoliation, thermal decomposition, un-zipping CNTs, plasma-enhanced chemical vapor deposition, and thermal chemical vapor deposition.(Choi et al. 2010)(Zhu et al. 2010) The physical properties of Graphene can be affectively tuned for a desired application by changing the mentioned methods and synthesis conditions.(Wu et al. 2018) Up until now, several characterization techniques have been used for spectroscopic characterization of graphene. However, Raman spectroscopy has been widely used as a characterization

technique for graphene owing to the easy determination of the dimensionality, the number of layers, crystal edge structure, and doping of graphene.

1.1.1. Raman Spectroscopy of Graphene

Raman spectroscopy discovered by C. V. Raman in 1928 is a standard, non-destructive spectroscopic technique used for crystals, semiconductors, and for molecules to analyze vibrational modes of the structures. Different from the Rayleigh Scattering where photons are elastically scattered, Raman spectroscopy, known as Raman scattering or Raman effect, depends on inelastic photon scattering. The molecular vibrations of the system is affected by the incident laser light, phonons or other excitations, causing the laser photons' energy to be moved up or down in the spectrum. The energy change offers information on the vibrational modes in the system. The Raman spectroscopy is a quite efficient technique for the characterization of graphene. The technique can reveal dimensionality, the number of layers(Malard et al. 2009), crystal edge structure(Solomon 1980), and doping.(Ferrari 2007)

In graphene, the excitation of laser causes the two main peaks in the raman spectrum; first in plane vibrational mode is G peak and the stacking order is 2D peak.(Kahl 2015) The positions of the peaks are typical for the characterization of graphene, the G peak is placed at 1580 cm^{-1} and the 2D peak is placed at 2690 cm^{-1}.(Saito et al. 2011) The given positions have been most of the time measured with the 532 nm excitation laser. The Raman spectrum will change with the number of graphene layers increase.(Ferrari 2007) The number of layer increment effect is also seen at the G band such as small red shift.(Malard et al. 2009) Although the 2D band of the monolayer graphene has a single sharp peak, AB-stacked the most stable form of bilayer graphene, that is overlapped half of the carbon atoms of two layers and it has a wider peak, which is composed of four peaks.(Partoens and Peeters 2006) Finally, 2D band of the multilayer graphene becomes even broader and looks like shouldered two peaks. Apart from determining the number of layers, Raman spectroscopy can also determine the doping level and defect of the graphene.(Beams, Gustavo Cançado, and Novotny 2015)

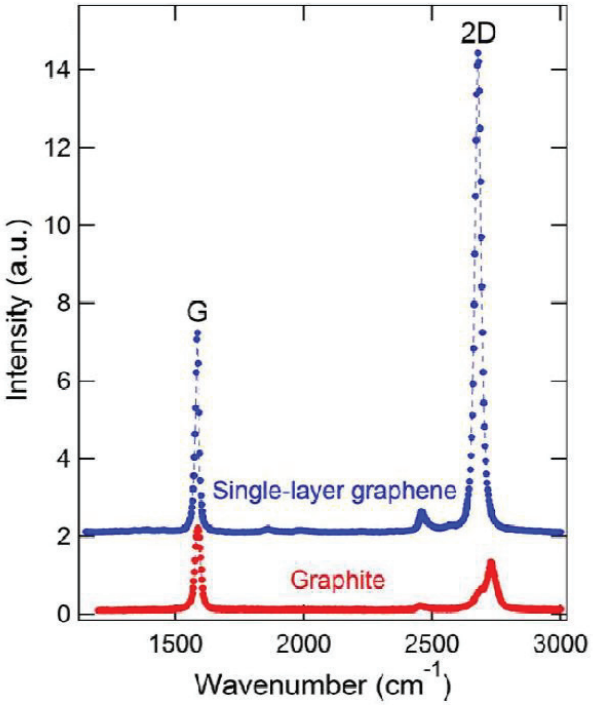

Figure 2. Raman spectra of graphene and graphite. The G and 2D bands reflecting the structural properties of the samples are clearly visible in the spectra.(Source : Kahl 2015) The relative intensities of G and 2D peaks give information about the bumber of graphene layers.

P-type or n-type doping changes the fermi surface of the graphene and hence the electrical and optical properties of graphene can be also changed. The existance of doping change can be identified with the Raman spectroscopy, the G peak of the graphene responds to the doping. A blueshift and narrow FWHM of the G band means that the doping exists in the graphene, but it can not give any information about doping types.(Tang, Guoxin, and Gao 2010) It also needs to be analyzed by 2D band for idenfiyng the doping type. Characterization of electron or hole type doping can be identified with the frequency shift of the 2D peak; the upshift of the peak means the hole doping wheras the red shifts of the peak means the electron doping.(Tang, Guoxin, and Gao 2010) As a result, the G and 2D peak position is a reliable method for the identifing the type (n-type or p-type) and quantity of doping (amount of doping).(Berciaud et al. 2008)

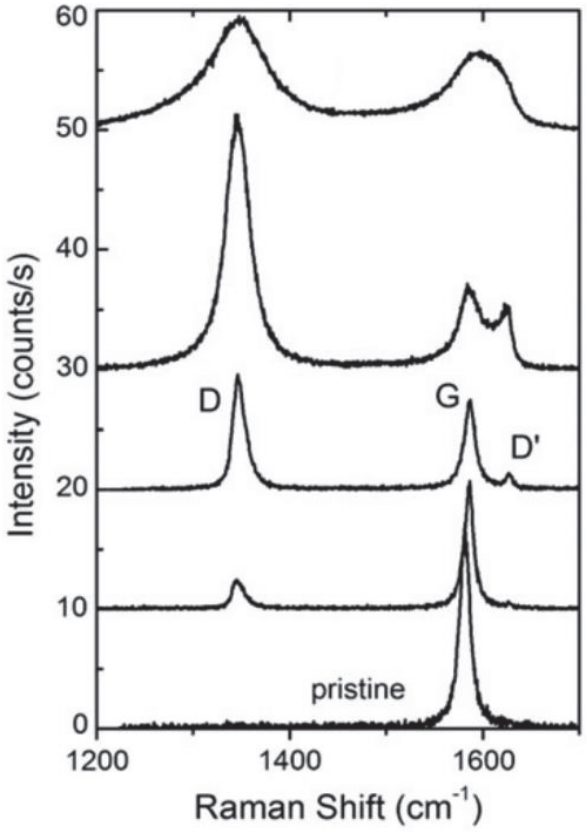

Figure 3. Raman spectra of the defective Graphene.
(Source : Beams, Gustavo Cançado, and Novotny 2015)

Raman spectroscopy can also identify the defect and the type of defect with the change of band intensitity and FWHM.(Das, Chakraborty, and Sood 2008) The point defect is generally known as the symmetry breaking that are due to the precence of vacancies, adatoms, and substitutional atoms. Non-defective graphene has no D band, so the D band will appear when the graphene lattice have defects.(Ni et al. 2008) The defect dose is directly related to the D band intensity, the increase of the defect dose causes the D band intensity increment and thus D band becomes evident near the G band.(Dresselhaus et al. 2010) In addition, the D band is also affected by the defect dose increment, the increment seems like convolution of the G and D band. For the maximum doping of the lattice, band peaks become broadened.(Dresselhaus et al. 2010)

1.1.2. Electronic Properties of Graphene

An ideal hexagonal honeycomb lattice structure of graphene has two C-C atoms in a unit cell with a length of 1.42 Å. In addition to that, carbon atoms have a constant rotation angle of 120°.(Weng et al. 2018) Each lattice of graphene has three strong localized σ bonds, and delocalized π bond in the perpendicular direction. Thanks to π bonds of graphene, freely moving π electrons provide a good electrical conductivity of graphene. The honeycomb lattice includes two sublattices, as mentioned by A site and B site.(Partoens and Peeters 2006)

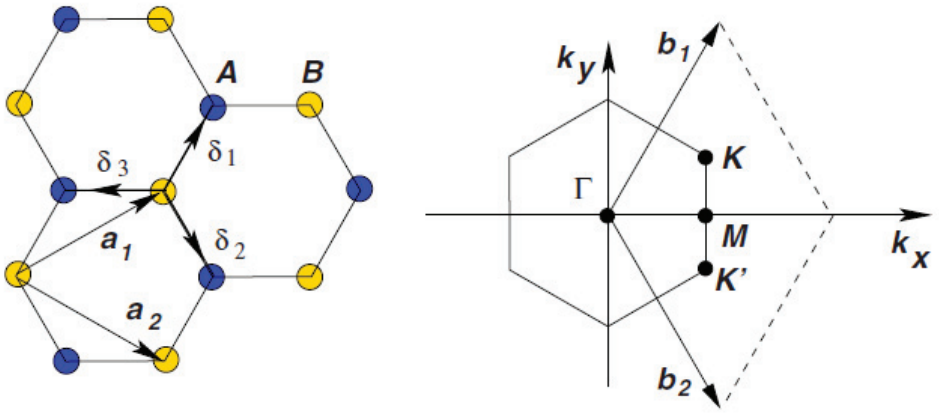

Figure 4. Honeycomb lattice of graphene and its Brillouin zone. The sp^2 hybridized carbon atoms make the graphene lattice. Each graphene unit cell contains two carbon atoms.

The lattice vectors a_1, a_2 and the reciprocal lattice vectors b_1, b_2 can be written as

$$a_1 = \frac{a}{2}(3, \sqrt{3}) \quad \text{and} \quad a_2 = \frac{a}{2}(3, -\sqrt{3}) \tag{1.1}$$

where a is the distance between the two carbon atoms in the lattice.

$$b_1 = \frac{2\pi}{3a}(1, \sqrt{3}) \quad \text{and} \quad b_2 = \frac{2\pi}{3a}\left(1, -\sqrt{3}\right) \tag{1.2}$$

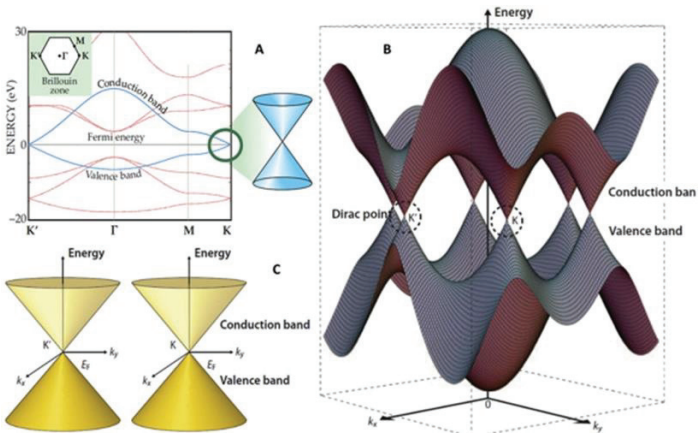

Figure 5. 2D and 3D band structure of graphene.
(Source : J. Wang et al. 2017)

The electronic band structure shows the zero energy gap of the graphene whose valance and conduction bands touch each other at two symmetric points that are **K** and **K'**, which is known as the Brillouin symmetry point. The positions in momentum space are

$$K = \left(\frac{2\pi}{3a}, \frac{2\pi}{3\sqrt{3a}}\right), \qquad K' = \left(\frac{2\pi}{3a}, -\frac{2\pi}{3\sqrt{3a}}\right) \tag{1.3}$$

The energy of the intersection point is linearly related to the wave vector. Therefore, the massless electrons and holes in graphene, they are called Dirac fermions and the crossing point is the Dirac point.(Avouris 2010) The individual carrier properties and the Dirac Fermi characteristic of graphene lead to the Quantum Hall effect where the Hall conductance of 2D electrons show quantized conductivity.
Additionally, approximated group velocity of charge carriers is $\mathbf{1 \times 10^6}\ {}^{\boldsymbol{m}}/_{\boldsymbol{S}}$ at the Dirac point.(Morichi et al. 2008) The Fermi level of defectless, freestanding, and undoped ideal graphene is expected to be at the Dirac point.(Avouris 2010)

The square root of the carrier density is directly proportional to the Fermi energy, $E_F \sim \sqrt{n}$.(Castro Neto et al. 2009) Therefore, by modulating the carrier density in graphene, the active tuning of the Fermi level is possible. As mentioned above, the carrier density can be changed by doping in several ways. Moreover, electrical, and optical properties of graphene can be affected by Fermi level, so many applications of graphene are directly related to the Fermi energy modulation.

1.1.3. Optical Properties of Graphene

The unique optical properties of graphene come from exclusive electronic band characteristic, which is the gapless band structure. Tunability of charge carriers with high mobility, and atomic thickness of graphene provide gate tuning of the optical properties.(Yan et al. 2007) Due to one atom thickness, graphene can yield immense optical absorption thanks to interband and intraband electronic transitions in graphene band structure.(Gan, Zhang, and Bao 2017)

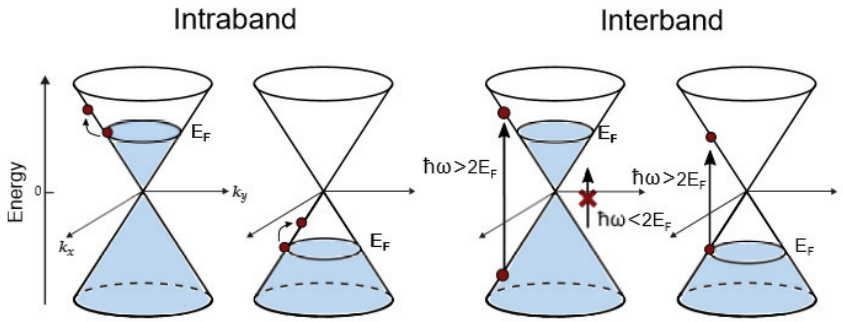

Figure 6. Intraband and interband electronic transitions in graphene.

(Source : Yakar 2020)

The intraband transition is an electronic transition in the same band. Conversely, the interband transition is a transition between the valance band and conduction band, it brings a ~2.3% absorption.(Li et al. 2008) A broadband absorption of graphene occurs in a broad range of range including the visible region too. The transmittance of graphene can be written as

$$T = \left(1 + \frac{1}{2}\pi\alpha\right)^{-2} \tag{1.4}$$

where α is the fine structure constant and $\alpha = e^2/\hbar c \sim 1/137$. (Nair et al. 2008)

The Fermi energy is important for electronic transitions, also for optical properties. For $2E_F > E_P$, where E_P is the incoming photon energy and E_F is Fermi energy,

interband transitions are not allowed, because of Pauli blocking.(Bao et al. 2014) If the photon energy is larger than Fermi energy such as $E_P > 2E_F$, interband transitions are allowed. The Fermi energy can be tuned by doping of graphene for making the interband transitions possible.(Sun et al. 2010) Consequently, the optical absorption can be altered by changing the Fermi energy.

Unlike the interband transitions, graphene has intraband transitions for $2E_f > E_p$ situation, which is at longer wavelengths and fall into the terahertz part of the electromagnetic spectrum. The terahertz spectrum causes graphene to behave like a conductive film, and the equation of optical conductivity for graphene is given by

$$\sigma(\omega) = \frac{\sigma_{DC}(E_F)}{(1 + \omega^2\tau^2)} \qquad (1.5)$$

where DC electrical conductivity is $\boldsymbol{\sigma_{DC}(E_F)}$, and the carrier momentum scattering time is represented by $\boldsymbol{\tau}$, and the photon frequency is the $\boldsymbol{\omega}$. In conclusion, the optical absorption of graphene can be tuned by manipulating the conductivity or the Fermi level of graphene for the area of application.(Sun et al. 2010)

1.2. Silver Nanowires

Transparent conductive electrodes have recently attracted great amount of attention with their widely use in new generation electronic devices. The high cost of transparent conductive electrodes, such as commonly used indium tin oxide (ITO), has led to the need for low-cost methods. For example, ITO is a fragile material, and it restricts the application area for flexible devices.(Tseng et al. 2020) Recent experiments have shown that silver nanowires (AgNWs) are promising nanomaterial for overcoming these problems. The most important difference is diffusive transmittance and specular transmittance of AgNWs when compared with ITO. In recent years, AgNWs have received increasing attention with their use in touch screen panels(Jo et al. 2016), solar cells(Jin et al. 2018), conductive electrodes(Meng et al. 2018), flexible electronic devices(Tseng et al. 2020), and conductive thin films(D. Li et al. 2018). Good electrical conductivity and mechanical flexibility of AgNWs are striking properties of AgNWs. The Ag NWs can be synthesized with various methods such as hydrothermal

method(Chen et al. 2010), electrochemical techniques(B. S. Kim et al. 2017), wet chemical synthesis(Zhang et al. 2004), DNA template synthesis(Zhao et al. 2009), and polyol process(Trung et al. 2017). In this thesis, a wet chemical method has been used for the synthesis of uniform thin and very long AgNWs. The synthetic method was used for long and thin nanowires in order to improve the performance parameters such as sheet resistance and optical transmittance of the transparent elctrodes fabricated on glass and flexible substrates. For instance, the transparent and large-area AgNW films have been developed with sheet resistances of less than 10 Ω/sq and 80%-90% transparency.(Cao et al. 2020) The AgNW density of the electrode directly affects the conductivity and transmittance of the electrode. Also, the length and diameter of AgNWs are very important parameters to improve transmittance (low) and conductivity (high).

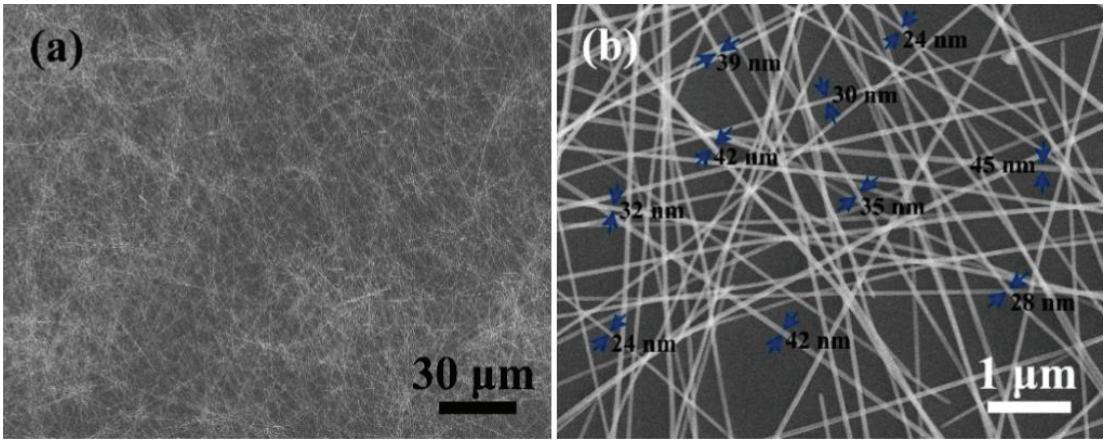

Figure 7. a) Low-magnification FE-SEM image of the synthesized AgNWs; and b) High-magnification FE-SEM image of the synthesized AgNWs.(Source : Y. Li et al. 2019)

The efficiency of the AgNW electrodes depends primarily on a bunch of features, including the structure of the nanowire such as length, diameter, size dispersity, and composition. The performance of AgNWs can be greatly improved by plasmonic welding, thermal annealing, and roll compression. These processes reduce contact resistance and increase the mechanical stability of the transparent conductive electrodes.(Cao et al. 2020)

1.2.1. Properties and Performance of the Silver Nanowire

Electrical characteristic of the AgNWs is extremely important for flexible conductive electrode. Due to the high electrical and thermal conductivities of bulk silver, AgNW is a very good candidate for flexible electrode applications.(Jia, Yang, and Zhang 2014) The sheet resistance of the AgNW is an important parameter for determining the electrical characteristic. The sheet resistance depends on the junction between AgNWs, and the distribution state of AgNWs. Indeed, high aspect ratio AgNWs is desirable for high performance transparent conductive electrodes.(Mutiso et al. 2013) Long wires with less contact means the low resistivity by reducing the contact resistance.(Mutiso et al. 2013)

Device fabrication method is a significant process that affects the sheet resistance and optical transmittance of the transparent conductive electrodes. The arrangements of the AgNWs directly affect the electrode conductivity performance, because of the connection between AgNWs. Due to polymer assisted synthesis, the surface of AgNWs has polymer residues that cause higher resistivity of the resulting fabricated conductive electrodes. Thermal annealing is a useful technique for solving the polymer residue problem of the AgNWs. It has been expermentally shown that the sheet resistance of the conductive electrode has been significantly decreased after annealing of the AgNWs.(Lagrange et al. 2015)

The transparency of the conductive electrode is a very strong indicator for the applications of fexible transparent electrodes in optoelectronic devices. The critical parameter is haze factor that is the ratio of diffuse transmission to direct transmission of the light, haze factor = scattered light/transmitted light.(Langley et al. 2013) The distribution of the AgNWs on the substrate will affect light transmittance of the electrode. Also, light transmittance is directly related to density of the AgNWs. The increase of AgNW density causes a decrase in the transmittance of the incoming light.(Hu et al. 2010) In conclusion, the highest transmittance and lowest resistance are strongly needed for the ideal transparent conductive electrodes.

1.3. Transition Metal Dichalcogenides

Two-dimensional materials have attracted enormous attention after the discovery of graphene, which is a one-atom thick sheet of carbon. Atomically thin two-dimensional transition metal dichalcogenide materials share some similarities with graphene. The similarities are the composition of the lattice structure as a single atomic layer with hexagonal arrangement and the Van der Waals interaction between layers. The most important difference between a TMDC and graphene is the electronic band gap.(Castro Neto et al. 2009) Unlike graphene, TMDCs have a band gap and the band gap condition is changed by the layer number.(Chaves et al. 2020) While the bulk TMDCs have indirect band gap, monolayer TMDCs have direct band gap. The energy bandgaps of TMDC types range from infrared to visible energy spectrum. A bulk TMDC crystal has a bandgap of around 1.1 eV but monolayer TMDCs can further increase to 1.5-2.2 eV.(Chhowalla et al. 2013) Despite the carrier mobility of TMDC is not as good as that of graphene, the TMDCs can reach high carrier mobility levels. All of these unique electronic properties make TMDCs promising candidate for next generation atomically thin device applications.

1.3.1. Crystal Structure of TMDCs

TMDCs are semiconductor materials and they can be represented generally with the chemical formula $\mathbf{MX_2}$, where M represents transition metal atom and X is a chalcogen atom (S, Se or Te). The layered structure of TMDC, X-M-X, is a sandwich-like structure that metal atoms are in between the two-layer of chalcogen atoms.(Chhowalla et al. 2013) The monolayer TMDC is only several Ångström thick. This reveals quantum confinement in the out-of-plane direction.(C. Lee et al. 2010) The tunable novel optical and electronic properties come from the quantum confinement, which can be tuned by an electric field, doping, and strain.(Chang et al. 2013) The surface of TMDCs is free of the dangling bonds and their structure is mechanically very robust. Moreover, Van der Waals interaction of TMDCs enables 2D materials to construct heterostructures without lattice mismatch. (Novoselov et al. 2016; Y. Liu et al. 2016; Jariwala, Marks, and Hersam 2017)

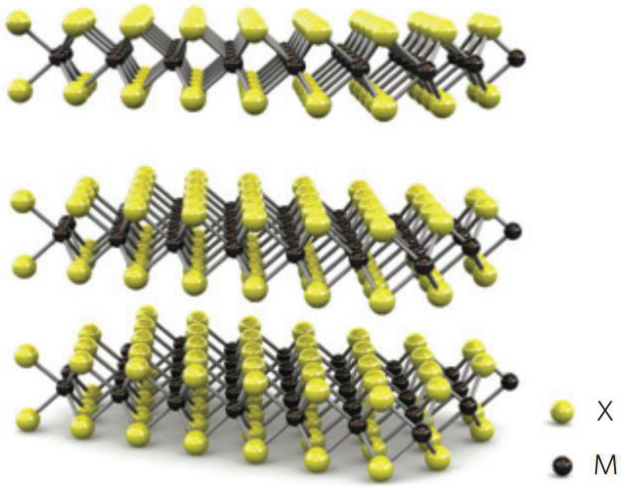

Figure 8. Crystal structure of TMDC.

(Source : Q. H. Wang et al. 2012)

The layered crystal structure arrangement of TMDC has three different types; the first is octahedral structure (1T phase), the second is trigonal prismatic structures (2H and 3R phases).(Toh et al. 2017) The crystal structure of TMDCs shows different properties: for instance, the 1T phase of TMDC reveals metallic-like properties whereas the other phases, 2H and 3R types, are semiconductors.(Datar, Bar-Sadan, and Ramasubramaniam 2020; Chia et al. 2015) Also, the application area can make use of the crystal structure of TMDC compounds. The 2H and 3R phases are more useful for electronic and optoelectronic applications with their stable crystal structure and semiconductor feature.

1.3.2 Electronic Band Structure of TMDCs

The electronic band structure of TMDC is highly important for tuning the optical and electronic properties. According to the evolution of thickness-dependent electrical band structure, TMDC can be used in many electronic and optoelectronic applications. The theoretical calculation of bulk 2H phase of MoS_2 shows the conduction band minimum is located at the middle of Γ and K point, and the valance band maximum

placed at the Γ point. Therefore, the bulk 2H phase of MoS_2 has an indirect band gap characteristic with a band gap of 1.2 eV.(Kuc and Heine 2015)

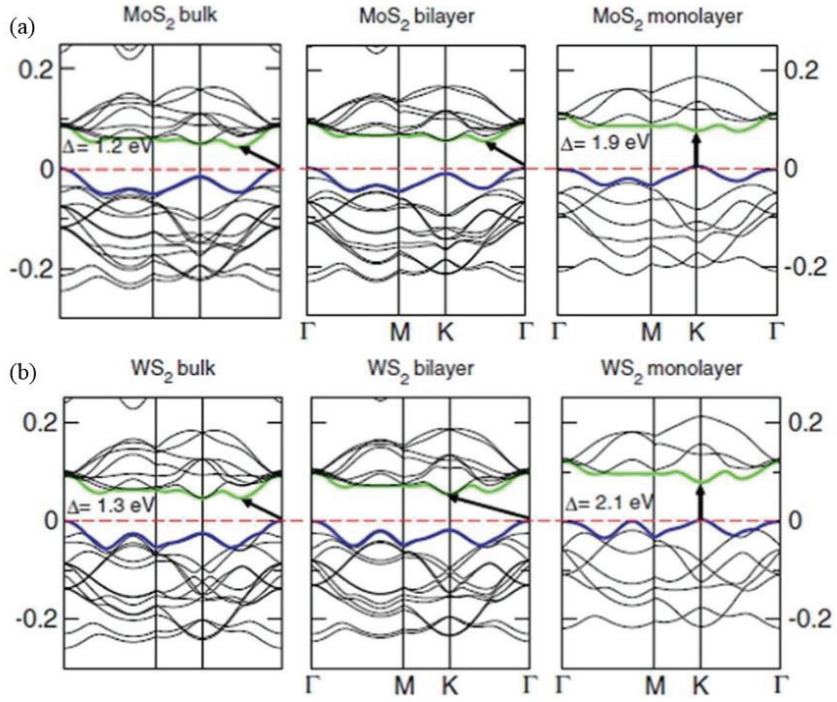

Figure 9. Electronic band structures of MoS_2 and WS_2 ; a)MoS_2, b)WS_2

(Source : Kuc and Heine 2015)

Theoretical calculations of the TMDC band structure show that the band structure changes as the material gets thinner. For example, when the MoS_2 gets thinner from bulk to monolayer, the band structure of MoS_2 becomes wider such as 1.2 eV to 1.9 eV.(Splendiani et al. 2010) The other TMDC materials such as WS_2, $MoSe_2$, WSe_2 have a similar indirect-to-direct band gap transition, when the TMDC material is monolayer. The motivations of the transition are orbital hybridization between P_Z orbitals of chalcogenide atoms and the *d* orbitals of the transition metals and the changes in coulombic interlayer interaction.(Chang et al. 2013) The direct bandgap exhibits strong photoluminescence (PL) emission in only monolayer TMDC.(Mak et al. 2010) The difference between the binding energy of excitons and bandgap corresponds to the optical bandgap. In addition, the large binding energy maintains the TMDC in a stable state even at room temperature, including strong PL intensity.(Berkelbach, Hybertsen, and Reichman 2013) However, PL profile of the monolayer TMDC is easily affected by

the environment such as underlying substrates, and gas molecules adsorbed by the surface of the TMDC crystal. The environmental effect can be identified with doping and strain, which influence emission peak wavelength and intensity due to the manipulation of the monolayer TMDC bandgap.(Conley et al. 2013; Ross et al. 2013; Mahmoodi et al. 2016)

1.3.3. Characterization Methods of TMDCs

Raman Spectroscopy

Raman spectroscopy, based on the Raman Effect, is a powerful and non-destructive technique for the characterization and analysis of TMDCs. Vibrational activity is measured for the individualization of the TMDCs by Raman active modes. Every TMDC has characteristic Raman active modes such as E_{2g}^{1} and A_{1g}.(Plechinger et al. 2012) The place of the mode peaks are used for identifying the TMDC, and peak amplitude is used for the estimation of the layer number. For example, MoS_2 has characteristic modes E_{2g}^{1} and A_{1g} at 387 cm^{-1} and 408 cm^{-1}, respectively.(Ganorkar et al., n.d.) Moreover, the distance between the two peaks denote the layer number of TMDC and that means the energy separation is used for identification of the TMDC monolayer.

Photoluminescence Spectroscopy

Photoluminescence is light emission of a material, which is a result of excited electron transition to a ground state. Photoluminescence spectroscopy is a measurement of emitted photons when these transitions occur. The radiative transitions are characteristic for each TMDC such as MoS_2 has a PL peak at 675.75 nm.(Ganorkar et al., n.d.) The advantage of a PL measurement is that it is non-invasive technique for determination of the optical bandgap of the material. Thanks to having direct bandgap of monolayer TMDCs, PL spectroscopy is a powerful and non-invasive tool for identifying monolayers.

Atomic Force Microscopy

Atomic force microscopy is a powerful characterization technique used to determine the surface morphology and thickness. The thickness of a TMDC crystal is directly related to the layer number and the surface morphology can give information about defects of the TMDC crystal. Atomic force microscopy has two commonly used modes, tapping mode and contact mode. The difference between these modes is the position of the cantilever. In the tapping mode the distance between the cantilever and sample is more than that in the contact mode. The measurement using the contact mode is more accurate, but it can be harmful for the sample. However, tapping mode is easier, non-destructive, and sufficiently accurate.

1.3.4. Molybdenum Disulfide

Molybdenum disulfide (MoS_2) is one of the most promising TMDC nanomaterial. MoS_2 has attracted great interest owing to its interesting electronic and optical properties. The physical properties MoS_2 are attractive because of the layer-dependent bandgap, which can be tuned with the number of layers.(Chhowalla et al. 2013; Chaves et al. 2020) MoS_2 monolayer is well-known for its electronic properties identified with the quantum confinement and surface effect. Besides, the semiconductive feature, the monolayer form has a direct bandgap that has radiative activity in the visible spectrum.(Conley et al. 2013) For instance, the energy bandgap changes from indirect ($\sim$1.29 eV) to direct bandgap ($\sim$1.80 eV) as the layer number decreases to monolayer. The direct bandgap of monolayer (1.8 eV) makes MoS_2 very attractive for switching nanodevice applications.(Kuc and Heine 2015) Mainly, Atomic force microscopy, Raman spectroscopy, and photoluminescence spectroscopy have been used for spectroscopic characterization of MoS_2. The distance between Mo and S atoms is approximately 2.41 Å and each layer is known as about 3.15 Å thick.(Ataca, Şahin, and Ciraci 2012) The distance information can be used to characterize the layer number of MoS_2 by using AFM.

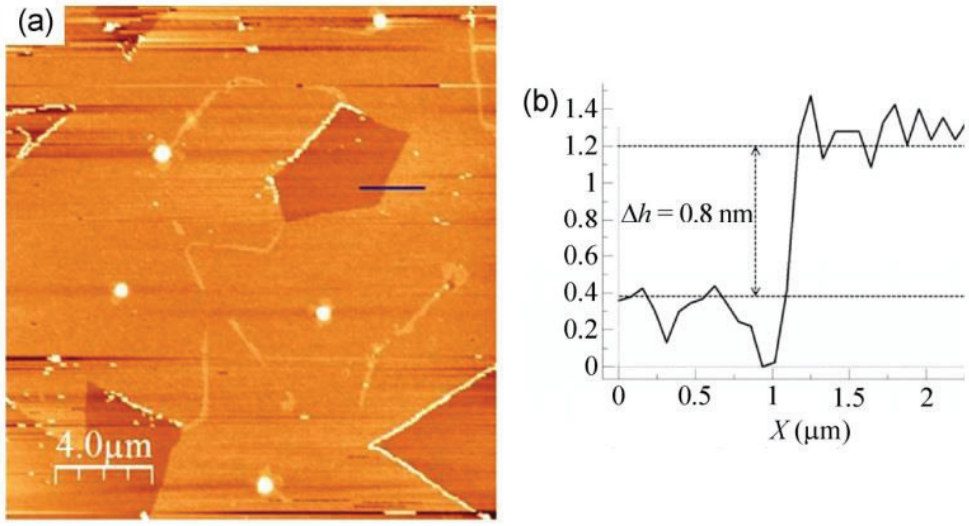

Figure 10. AFM characterization of MoS_2; a) AFM image of a grown MoS_2 monolayer film,b) height profile of the MoS_2 thin film. (Source : Senthilkumar et al. 2014)

The unique vibrational modes of MoS_2 placed at 387 cm^{-1}, 408 cm^{-1} that are E^1_{2g} and A_{1g}, respectively. The in-plane vibrational mode is E^1_{2g}, which is caused by the vibration of Mo and S atoms. The out-plane mode is A_{1g}, which results from the vibration of S atoms. The thickness of the MoS_2 film affects these two modes, and the frequency distance between modes of the peaks can give information about the film as a monolayer. The frequency difference is around 19.5 cm^{-1} for the monolayer MoS_2.(Splendiani et al. 2010)

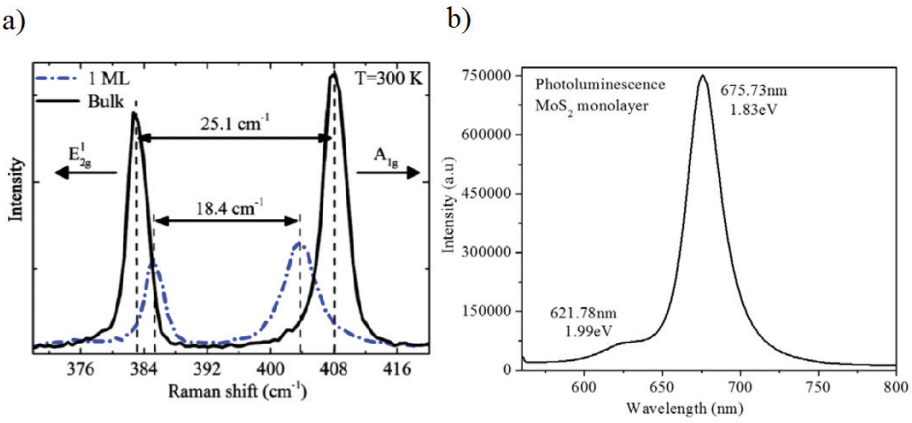

Figure 11. Raman and PL spectra of MoS_2; a) Raman spectra of different layer number, b) PL spectrum of monolayer MoS_2.(Source : Splendiani et al. 2010; Ganorkar et al., n.d.)

Photoluminescence spectroscopy is a non-destructive, contactless method for characterizing the electronic structure of nanomaterials. The working principle of photoluminescence spectroscopy is based on the photoexcitation principle. Photoexcitation causes electrons to move to the excited state. When the electrons return to the ground state, there can be emitted light or may not. The emitted light is related to the energy difference between the ground state and excited state. The number of layers is closely related to the photoluminescence of MoS_2.(Mak et al. 2010) The photoluminescence peaks are distinct for different number of layers. Two characteristic absorption peaks of monolayer MoS_2 are placed at 670 *nm* and 672 *nm*, which are identified as A1 and B1 exciton peaks.(Splendiani et al. 2010; Ganorkar et al., n.d.) The energy split from the valance band spin-orbit coupling implies the excitons.

1.3.5. Tungsten Disulfide

The other similar structured TMDC is a tungsten disulfide (WS_2). In contrast to graphene, tungsten disulfide offers great promise for electronic and optical devices with layer-dependent tunable electronic bandgap. Also, superior carrier mobility and chemical robustness of WS_2 makes it desirable for a variety of critical applications in electronics and photonics.(Q. H. Wang et al. 2012) A monolayer WS_2 consists of hexagonal lattice structure with metal atom layer, which is sandwiched between sulfur atom layers. While bulk tungsten disulfide has an indirect band gap of 1.3 eV, monolayer WS_2 has a direct band gap of 2.1 eV.(L. Liu et al. 2011) The most obvious

difference of monolayer tungsten disulfide from other TMDCs, WS_2 has a strong photoluminescence emission.(Kang, Godin, and Yang 2015) The important exhibition of WS_2 is strong spin-orbit coupling and band splitting owing to the spin enabling spintronics.(Gao et al. 2015) WS_2 can also be used in many application areas such as sensors, photodetectors, field effect transistors, thanks to its characteristic optical and electrical properties. The characteristic features of a WS_2 are important for the intended application area. The characterization techniques for WS_2 are optical microscopy, Raman spectroscopy, photoluminescence spectroscopy, and atomic force microscopy techniques.

Raman spectroscopy is a powerful technique for identifying the quality and thickness of WS_2. Tungsten disulfide has two characteristic Raman active modes that are E_{2g}^1 and A_{1g}. The peak locations differ due to the layer number, while the peaks of bulk WS_2 are at 348.7 cm^{-1} and 419.1 cm^{-1}. The peaks of monolayer WS_2 are at 352.1 cm^{-1} and 417.5 cm^{-1}.(Qiao et al. 2017) The distance between the two characteristic peaks in the Raman spectrum indicates whether the WS_2 is monolayer or bulk. Furthermore, the layer number of the WS_2 can be estimated by the Raman peak intensities.

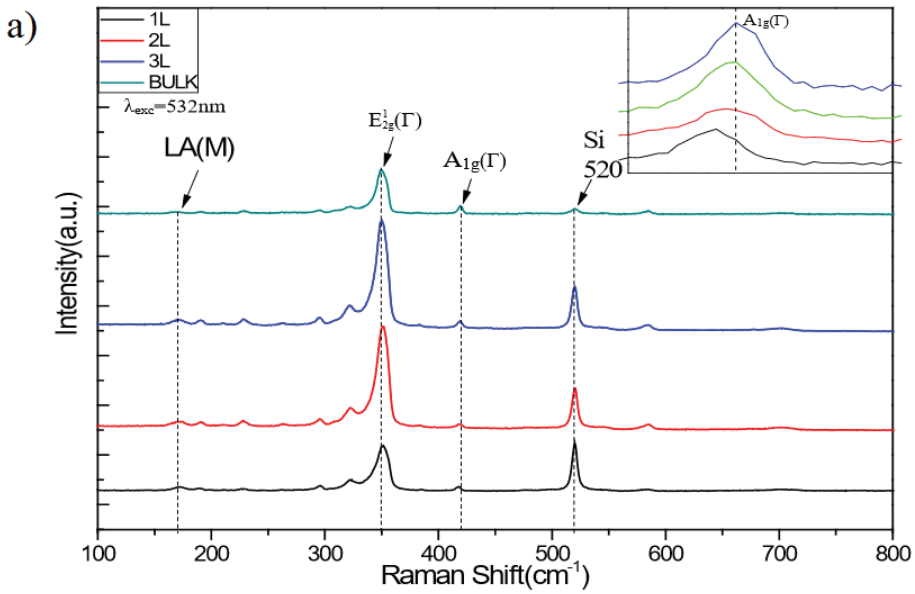

b)

	1-layer	2-layers	3-layers	Bulk
$E^1_{2g}(\Gamma)$(cm^{-1})	352.1	350.9	349.8	348.7
$A_{1g}(\Gamma)(cm^{-1})$	417.5	418.3	418.7	419.1

Figure 12. a) Raman spectra measurements; Raman shift of different layers of WS2
b) The frequency of the Raman shift as a function of the layer number.(Source : Qiao et al. 2017)

Owing to the direct bang gap of monolayer tungsten disulfide, photoluminescence emission has been observed in the PL spectrum. Photoluminescence of WS_2 is indeed very strong and hence the PL spectrum can be measured for the characterization of the WS_2. The only exitonic PL peak is located at $\sim 620\ nm$ and, in fact, it proves that WS_2 is monolayer. (Lan et al. 2018)

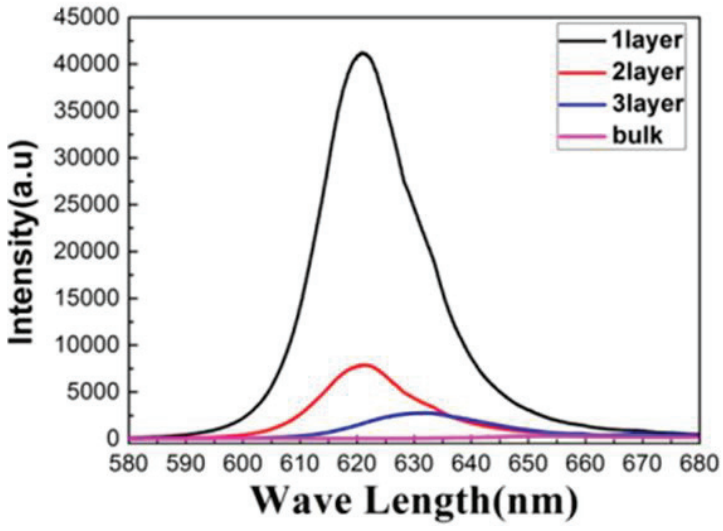

Figure 13. PL spectra of bulk, one-layer, two-layer, and three-layer tungsten disulfide.

The thickness of the crystal can give very important information about layer number, and the thickness can be measured by using atomic force microscopy. The distance between the tungsten and sulfur atoms is around 2.39 Å and the thickness of the WS_2 is around 3.13 Å for each layer. Atomic force microscopy also shows the lateral size and structural defects of the crystal.(Ataca, Şahin, and Ciraci 2012)

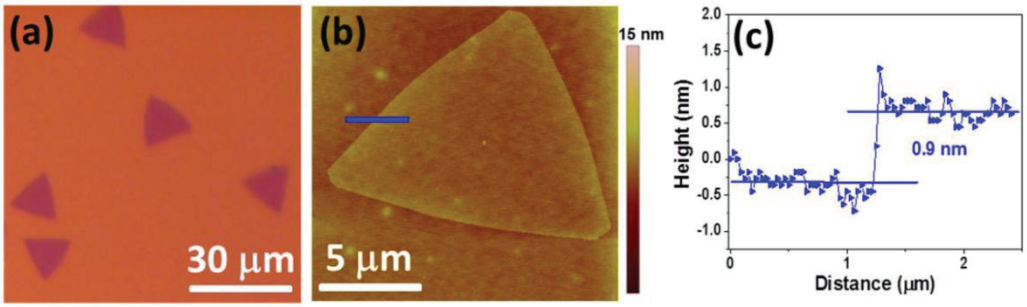

Figure 14. (a) Optical microscopy image, (b) AFM image, and (c) Height profile of WS_2.(Source : Khairuzzaman 2016)

CHAPTER 2

EXPERIMENTAL METHODS AND RESULTS

2.1. Synthesis and Transfer of Graphene

Graphene can be prepared and synthesized by using a variety of techniques such as exfoliation, thermal decomposition, un-zipping CNTs, plasma enhanced chemical vapor deposition, and thermal chemical vapor deposition. The most promising and scalable technique for the growth of graphene is thermal chemical vapor deposition. In this thesis, CVD growth procedure was used as following the previously published graphene synthesis procedure by Salihoglu et al. 2016. The furnace with a 9 in. diameter quartz tube and Cu foils with a thickness of 25 µm were used for the synthesis of single layer graphene on copper foils. After placing Cu foils, the quartz tube was evacuated, because low pressure is needed for the growth process. After evacuation, the furnace was heated to 1035 °C. The partial pressures $\boldsymbol{P_{CH4}}$ and $\boldsymbol{P_{H2}}$ are 1.5 Torr and 3.5 Torr, respectively. The flow rate of the promoter gases were J_{CH4}, = 10 s.c.c.m and J_{H2} = 85 s.c.c.m.,

which were used for the full coverage of single layer graphene on copper foils. The growth time was 10 min for the process. After the growth, the samples were cooled down to the room temperature naturally. It should be noted that the ends of the quartz tube was cooled during the annealing step in order to protect plastic O-rings.

The transfer of graphene from copper foil to any other substrate can be done with wet transfer. First, graphene grown on Cu foil was covered by the photoresist with a drop coating method. Photoresist coated samples cured at 65 °C overnight. The Cu foil was etched in an etchant solution of a 1 M iron chloride solution. Subsequently, photoresist/graphene layer was rinsed in deionized water for the cleaning the chemical residue left on graphene. Cleaned photoresist/graphene layer was carefully placed on the target substrate. A hot plate at 75 °C used for the composing of the photoresist/graphene layer to the target substrate for a minute. Lastly, the photoresist layer was washed with acetone, isopropyl alcohol, and deionized water, and then dried with a stream of nitrogen.

2.2. Synthesis and Transfer of TMDC

TMDCs can be synthesized with a variety of techniques such as exfoliation, wet chemistry, and chemical vapor deposition. In this thesis, the two-zone CVD method was used for the synthesis of TMDs, molybdenum disulfide and tungsten disulfide. The two methods for the synthesis of MoS_2 and WS_2 have a very similar process. They differ with the powder amount, and also temperature depending on the type of the powder. The optimization of the process for synthesizing MoS_2 and WS_2 was done by following the published work by F. Zhang et al. 2019.

Table 1. CVD synthesis parameters of MoS_2 and WS_2.

	Temperature	**Ar Flow**	**MoO_3/WO_3**	**S**
MoS_2	**780**	**100 s.c.c.m.**	**15 mg**	**200 mg**
WS_2	**825**	**100 s.c.c.m.**	**10 mg**	**200 mg**

2.3. Synthesis and Transfer of Molybdenum Disulfide

A powder-based atmospheric pressure CVD method in an inert atmosphere was used for the synthesis of MoS_2. One of the quartz boats with a powder mixture of 15 mg (the ratio 5:1) MoO_3 and NaBr was carefully placed at the center of the furnace, and then the other quartz boat with a 200 mg sulfur powder was placed in the furnace at 200 °C. A 300 nm Si/SiO_2 substrate was placed face down on the quartz boat that has the Mo source. The SiO_2 substrate was carefully cleaned in a Piranha solution, which is a mixture of concentrated sulphuric acid with hydrogen peroxide in a ratio of 3:1 to 6:1 *(Caution: piranha solution reacts very violently with organic maters.)*. Firstly, the furnace was flushed with excess amount of Ar gas, 1000 s.c.c.m Ar, for 15 minutes. The furnace was heated to 780 °C in 30 min. During the whole growth process, 100 s.c.c.m. Ar flow was used as a carrier gas. After the furnace reaches to 780 °C, around 15 minutes is enough for the deposition of the MoS_2 flakes. Finally, the furnace was opened completely for finishing the growth of MoS_2, and Ar flow was continued to cool down the hot furnace.

As also commonly used in the literature, a PMMA assisted wet transfer method was used for the transfer of MoS_2 to the target substrate. First, a PMMA layer was spin-coated on the as grown MoS_2 for 2 minutes at 2000 rpm, and then it was baked at 130 °C for 3 minutes. A PMMA covered $MoS_2/Si/SiO_2$ substrate was immersed in 2 M NaOH solution on hot plate at 100 °C. After the etching of SiO_2, PMMA/MoS_2 layer was put into DI water with a fishing out technique. The DI water was used for cleaning any residue of the etcher solution. Subsequently, PMMA/MoS_2 layer was placed on the target substrate and it was baked for around 5 min at 200 °C for drying. Finally, the PMMA layer was washed with acetone and isopropyl alcohol.

2.4. Synthesis and Transfer of Tungsten Disulfide

A similar process used for the synthesis of MoS_2 was used for the synthesis of tungsten disulfide, WS_2. The main differences were the temperature of the annealing furnace and the powder amount used for the deposition of metal and Sulphur sources. The furnace was heated to the 825 °C in 30 minutes. The powder amounts were 10 mg WO_3 and NaBr with the ratio 5:1 and 200 mg sulfur. The Sulfur needs the same

temperature of 200 °C for the growth. The transfer of WS_2 is very similar to the transfer process used for MoS_2, as can be read above.

2.5. Synthesis and Purification of Silver Nanowire

All chemicals were used without any further purification as they were obtained. The PVP was dissolved in a solution of 10 mL glycerol and an amount of EG for a standard synthesis. Meanwhile, in 5 mL of glycerol solution, 0.034 g of $AgNO_3$ was dissolved. The glycerol and $AgNO_3$ solution added to flask for the heating in oil bath. Then the oil bath heated to 170 °C in 30 minutes with stirring the solution. An amount of catalysts ($CuCl_3$, $CoCl_3$, $MnCl_3$, and $CrCl_3$) solution was added drop wisely to the solution. At the end of the two hours, the synthesized AgNW solution was cooled down fastly with an ice bath.

For the purification of AgNWs, the solution was diluted with 30 mL of deionized water. Acetone (80-160mL) was dripped into it by stirring slowly, while the nanowires were clustered. It was waited for 10 minutes for the particles to settle to the bottom of the bottle and the supernatant on top was replaced with a pipette. 0.5% PVP was added into 20 mL of distilled water, the clustered nanowires were re-dissolved in this water, 40-80 ml of acetone was added to precipitate and this procedure was repeated 4 times to obtain high purity nanowires. Finally, the nanowires were dispersed in ispopropyl alcohol, and then the nanowires were centrifuged and recovered from the excess PVP.

2.6. Optical Measurements

Optical transmission of AgNW thin films and the quality (length, diameter, and distribution on the surface after coating) of AgNWs were tested by using a spectrophotometer, an optical microscope, and a scanning electron microscope. The nanowire length and diameter directly affect the transmission performance of the electrode fabricated from silver nanowires. Thinner and longer nanowires were expected for the maximization of the transmission of the nanowire electrode. The transmission of the electrodes is around ~87% and the graphene effect on the transmission is ~2.5%. Optical properties of the electrodes will be discussed in the result and discussion section.

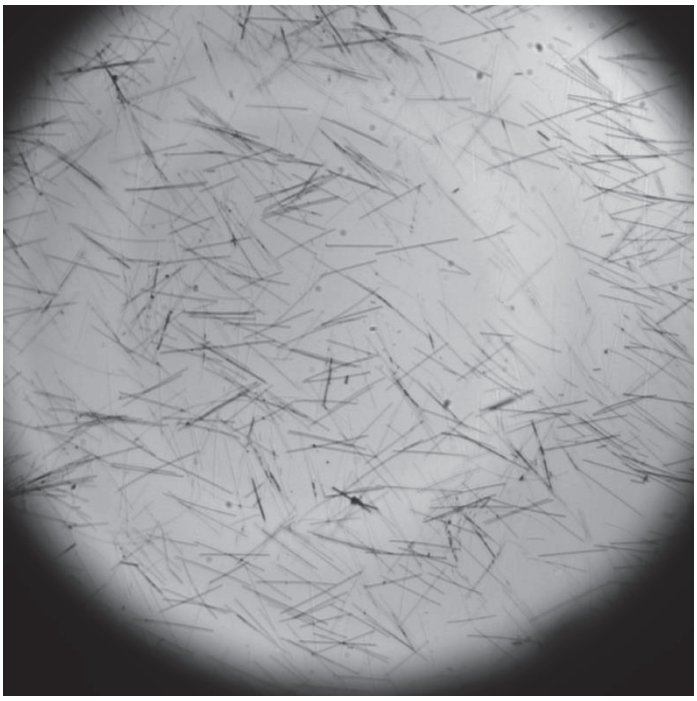

Figure 15. Optical microscopy image of Co catalyzed AgNWs on a glass substrate.

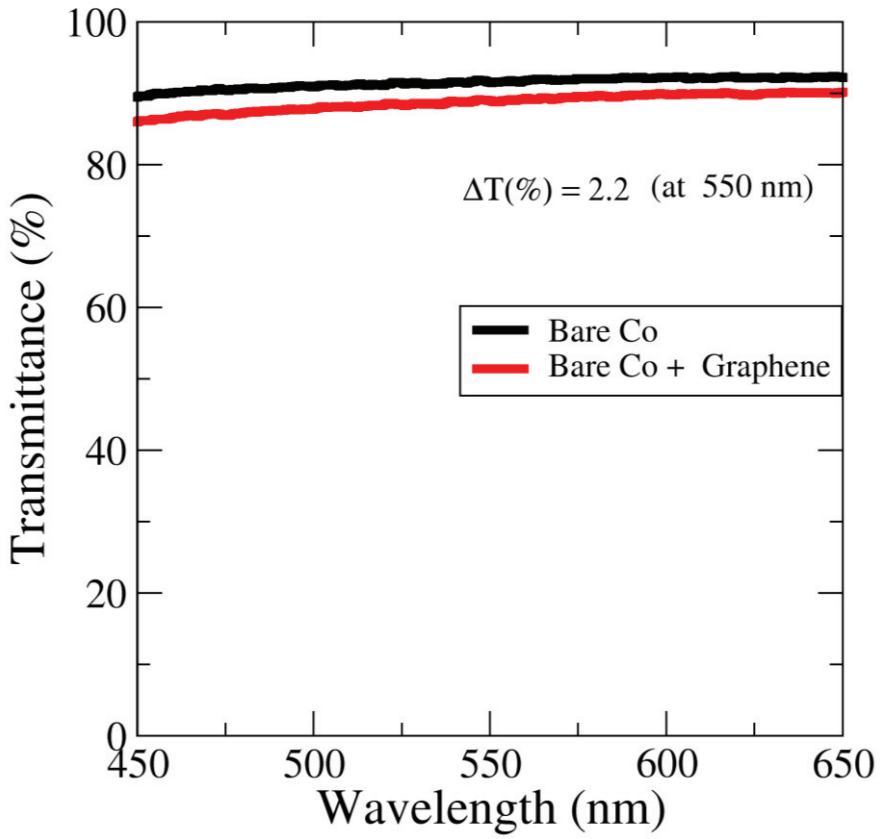

Figure 16. Transmittance of the Co catalyzed electrode containing Ag nanowires on a glass substrate.

The black curve indicates transmision of the transparent conducting electrode fabricated from Co catalysed Ag NWs. The red curve shows transmision of the graphene coated transparent electrode fabricated from Co catalysed Ag NWs. The decrease in transmision in the graphene coated transparent electrode is due to the interband transitions in graphene in the visible region of the electromagnetic spectrum.

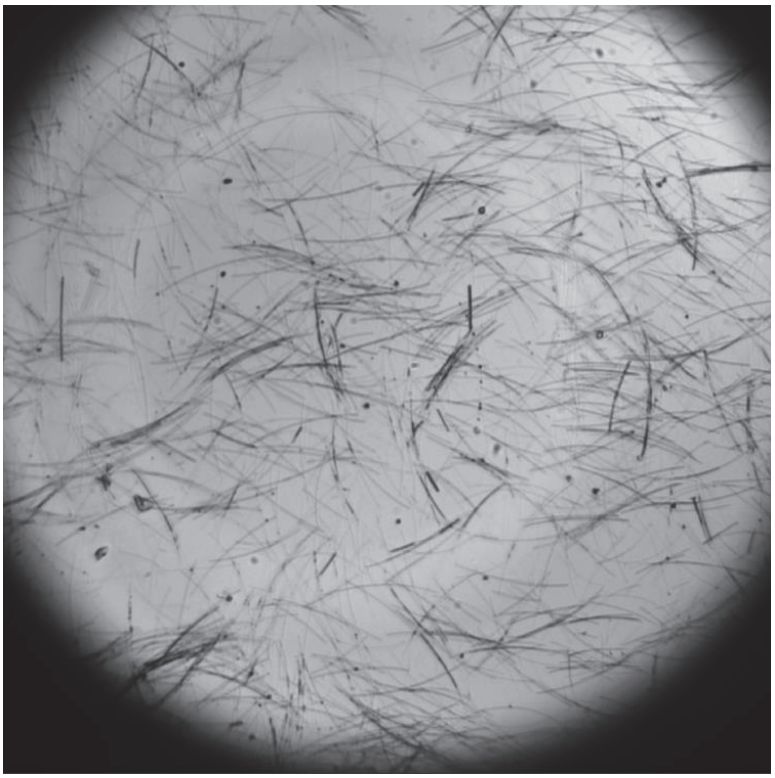

Figure 17. Optical microscopy image of Cr catalyzed AgNWs coated on a glass substrate.

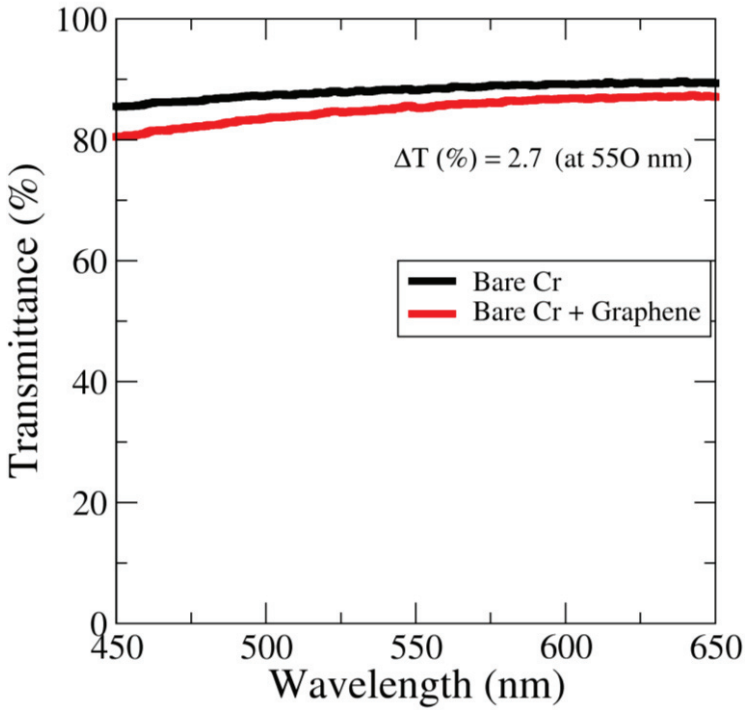

Figure 18. Transmittance of the Cr catalyzed electrode containing Ag nanowires on a glass substrate.

The black curve indicates transmision of the transparent conducting electrode fabricated from Cr catalysed Ag NWs. The red curve shows transmision of the graphene coated transparent electrode fabricated from Cr catalysed Ag NWs. The decrease in transmision in the graphene coated transparent electrode is due to the interband transitions in graphene in the visible region of the electromagnetic spectrum.

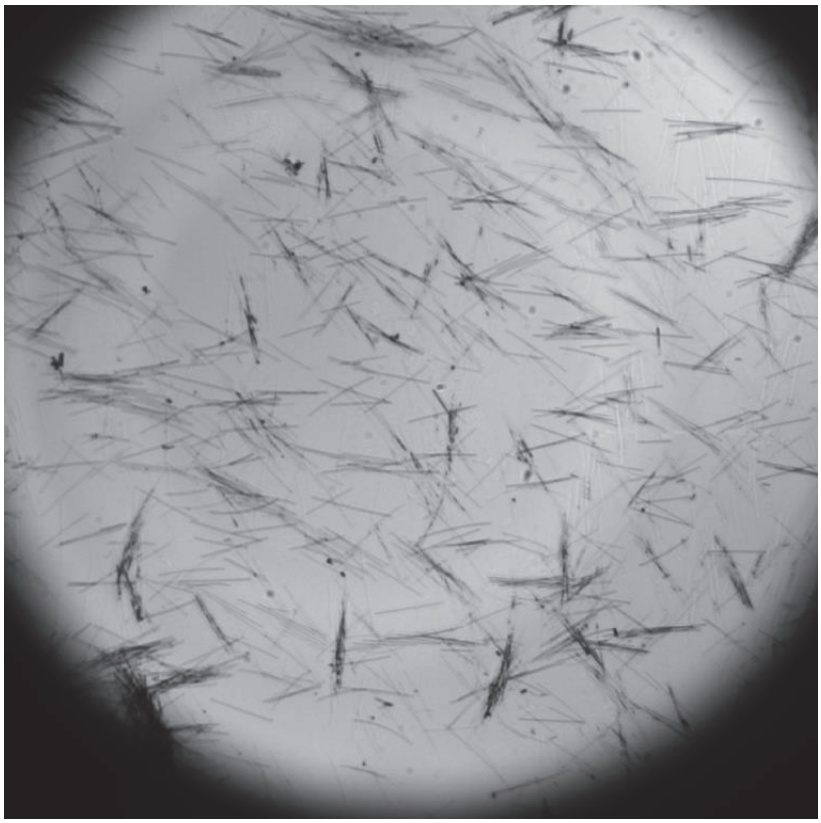

Figure 19. Optical microscopy image of Mn catalyzed AgNWs on a glass substrate.

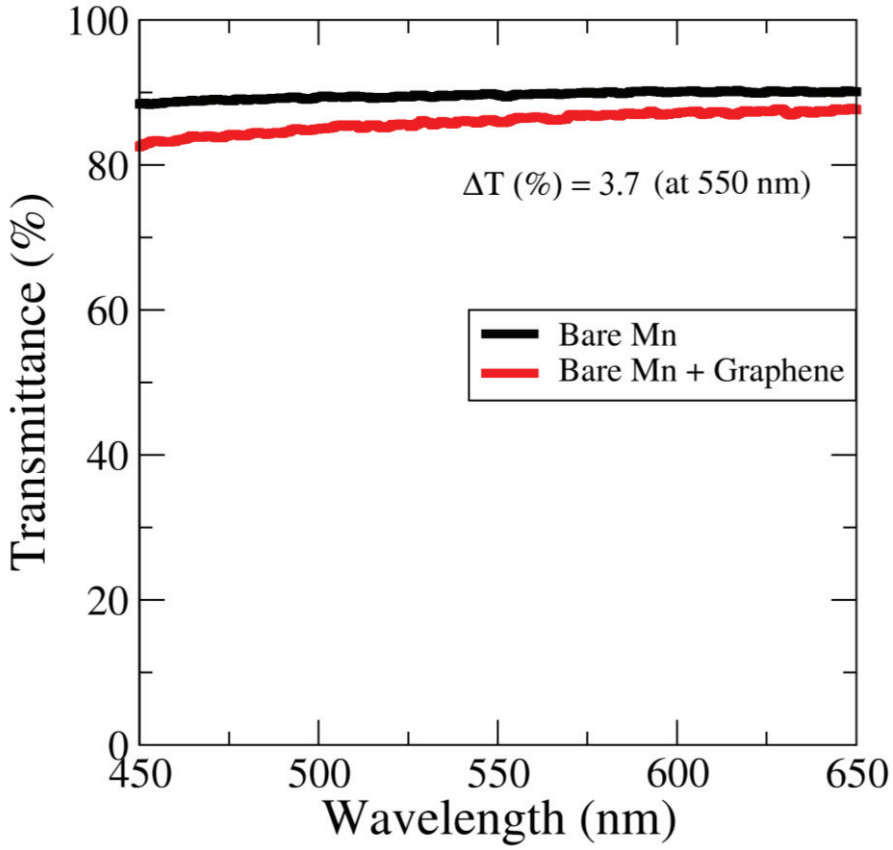

Figure 20. Transmittance of the Mn catalyzed electrode containing Ag nanowires on a glass substrate.

The black curve indicates transmision of the transparent conducting electrode fabricated from Mn catalysed Ag NWs. The red curve shows transmision of the graphene coated transparent electrode fabricated from Mn catalysed Ag NWs. The decrease in transmision in the graphene coated transparent electrode is due to the interband transitions in graphene in the visible region of the electromagnetic spectrum.

The black curve indicates transmision of the transparent conducting electrode fabricated from Cu catalysed Ag NWs. The blue curve shows transmision of the graphene coated transparent electrode fabricated from Cu catalysed Ag NWs. The red curve represents transmision of graphene and WS_2 coated electrode fabricated from Cu catalysed Ag NWs.

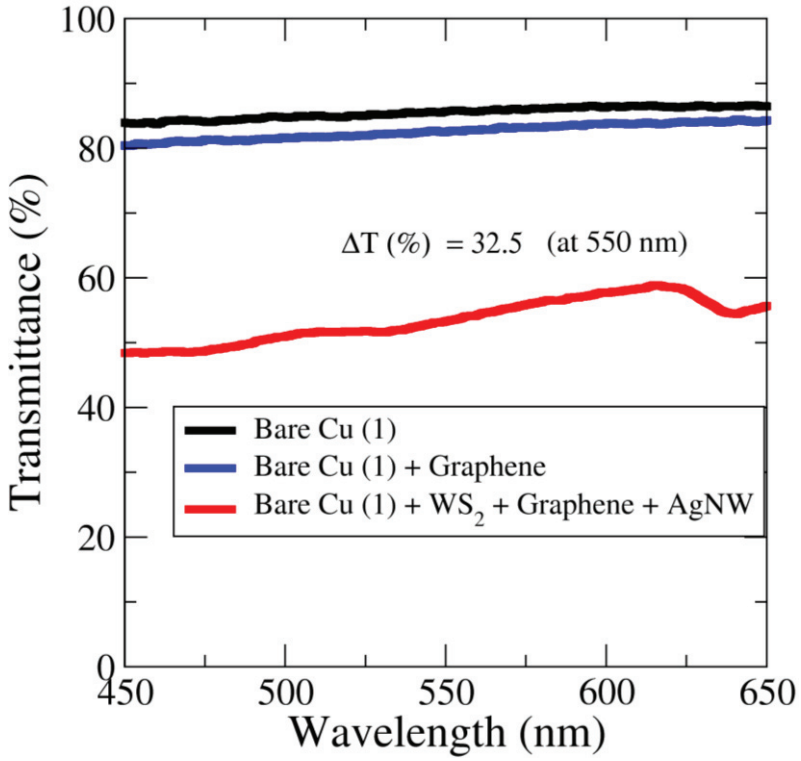

Figure 21. Transmittance of the Cu catalyzed electrode containing Ag nanowires, graphene and WS_2 on a glass substrate.

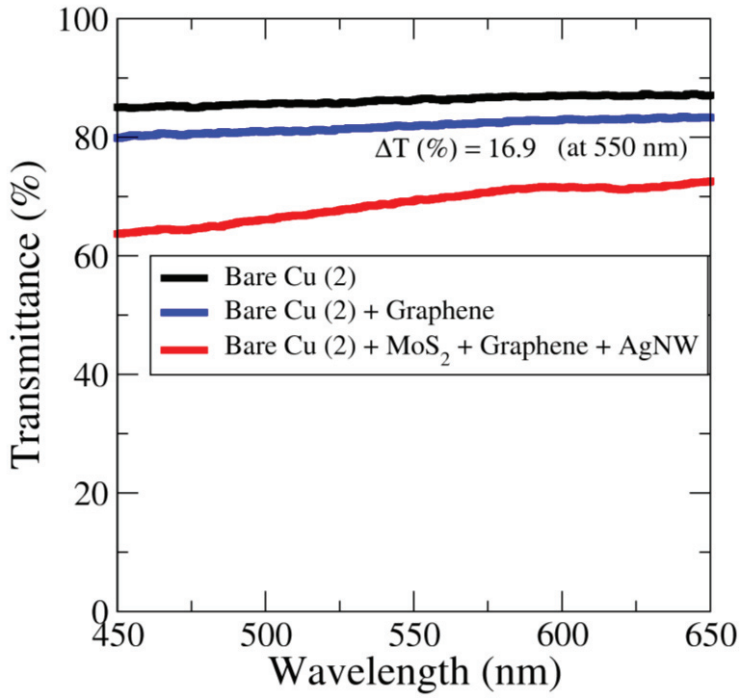

Figure 22. Transmittance of the Cu catalyzed electrode containing Ag nanowires, graphene and MoS_2 on a glass substrate.

The black curve indicates transmision of the transparent conducting electrode fabricated from Cu catalysed Ag NWs. The blue curve shows transmision of the graphene coated transparent electrode fabricated from Cu catalysed Ag NWs. The red curve represents transmision of graphene and MoS_2 coated electrode fabricated from Cu catalysed Ag NWs.

2.7. Electrical Measurements

The most important factor determining the electrical quality of the transparent conducting electrode is the sheet resistance of the electrode, a measure of resistance of conducting thin films. In this thesis, AgNW, graphene, and monolayer TMDC based transparent conducting electrodes were fabricated. The effect of variety of catalysts (Co, Cu, Mn, and Cr) in the synthesis of AgNWs was extensively studied for finding the best AgNWs for the transparent conducting electrodes. The length and diameter of the AgNWs are key parameters for determining the quality of the nanowires in the electrode fabrication. The sheet resistance of the electrodes fabricated from the AgNWs can give information about the electrical properties of the fabricated transparent conducting electrodes. The lowest resistance of the transparent conducting electrodes was expected for the highest conductivity of the electrodes. A multimeter was used to measure the resistance of the electrodes. The effect of annealing temperature on the resistance of the transparent conducting electrode will be discussed in the result and discussion section.

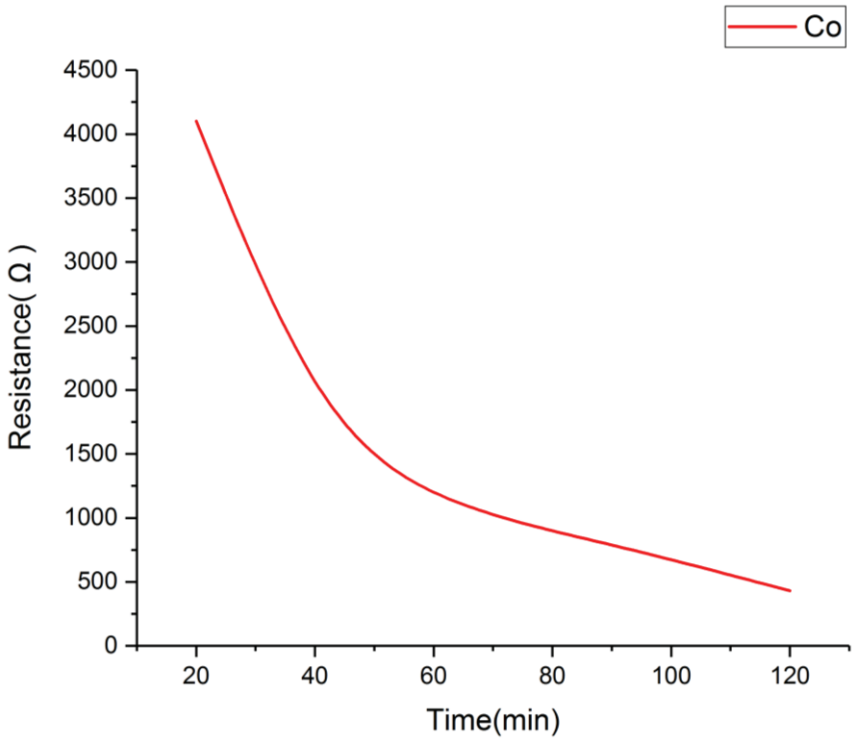

Figure 23. Resistance change of transparent conducting thin films fabricated by using Co catalyzed AgNWs with annealing time.

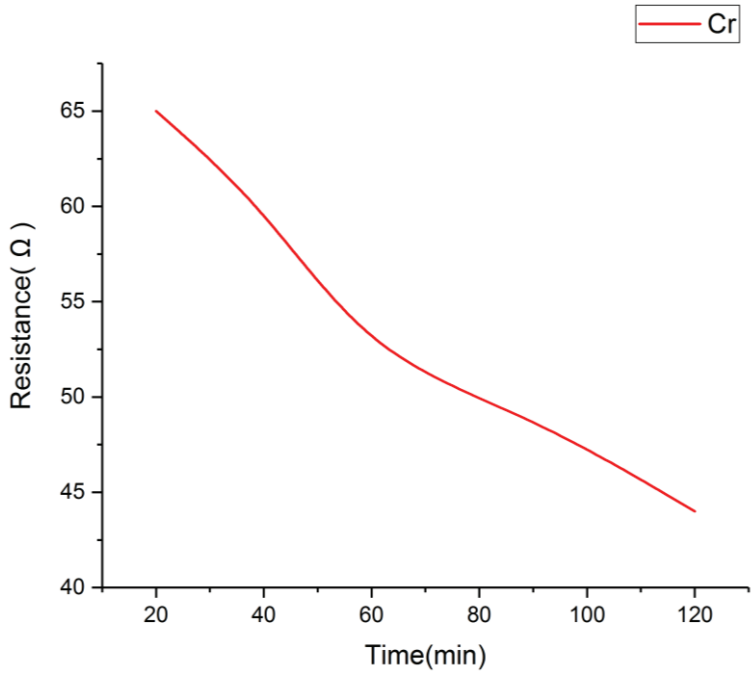

Figure 24. Resistance change of transparent conducting thin films fabricated by using Cr catalyzed AgNWs with annealing time.

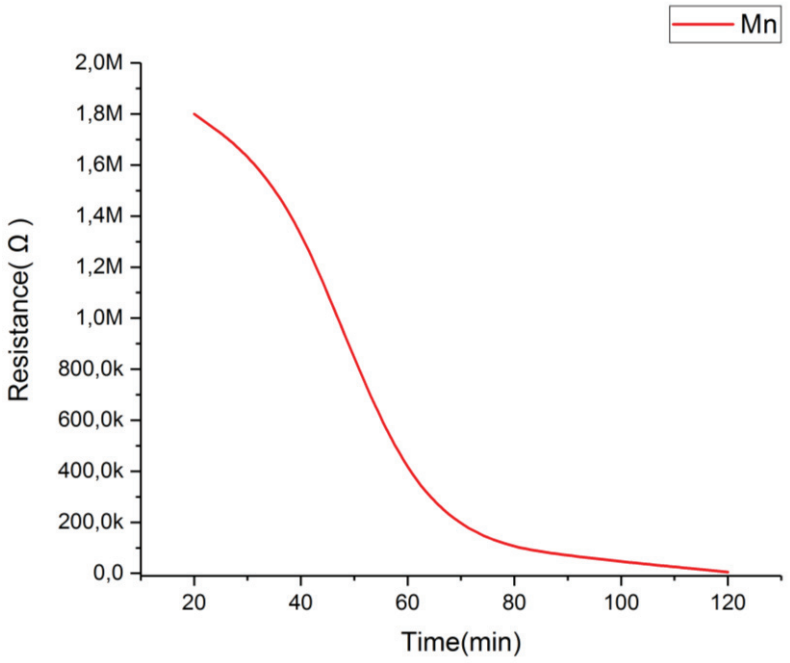

Figure 25. Resistance change of transparent conducting thin films fabricated by using Mn catalyzed AgNWs with annealing time.

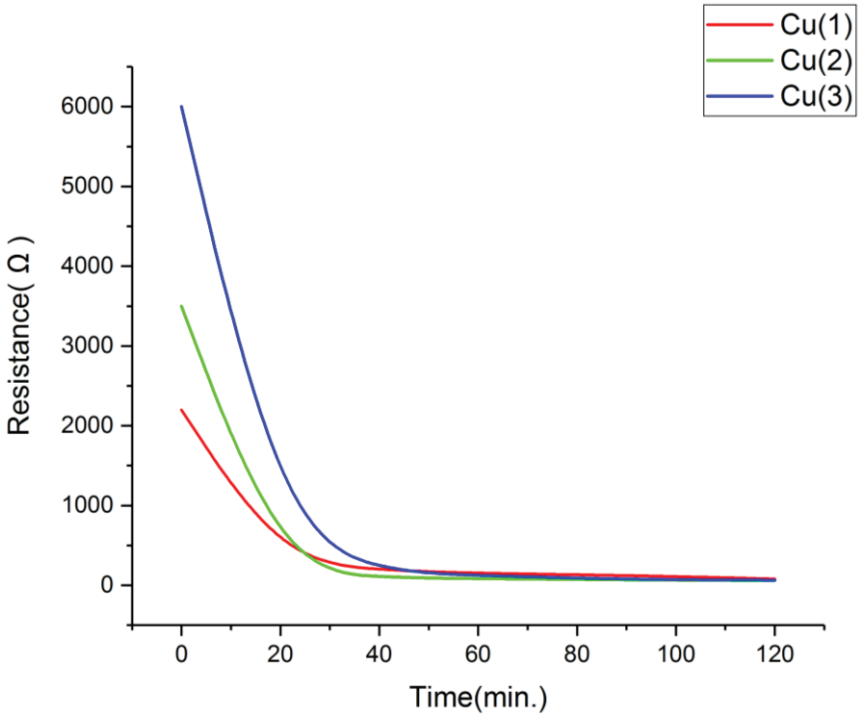

Figure 26. Resistance change of transparent conducting thin films fabricated by using Cu catalyzed AgNWs with annealing time.

The flexible and transparent conducting electrodes were fabricated on flexible substrates. The flexibility of electrodes was tested by the 90° bending test. The bending was done 90 times for four different flexible electrodes. The electrodes were fabricated from Ag NWs synthesized by using four different catalysts, namely $CuCl_3$, $CoCl_3$, $MnCl_3$, and $CrCl_3$. The bending effect is directly related to the length of the nanowires. The effect of bending will be discussed in the result and discussion section. Below in Figures 27-30, we provide the results obtained from the bending tests.

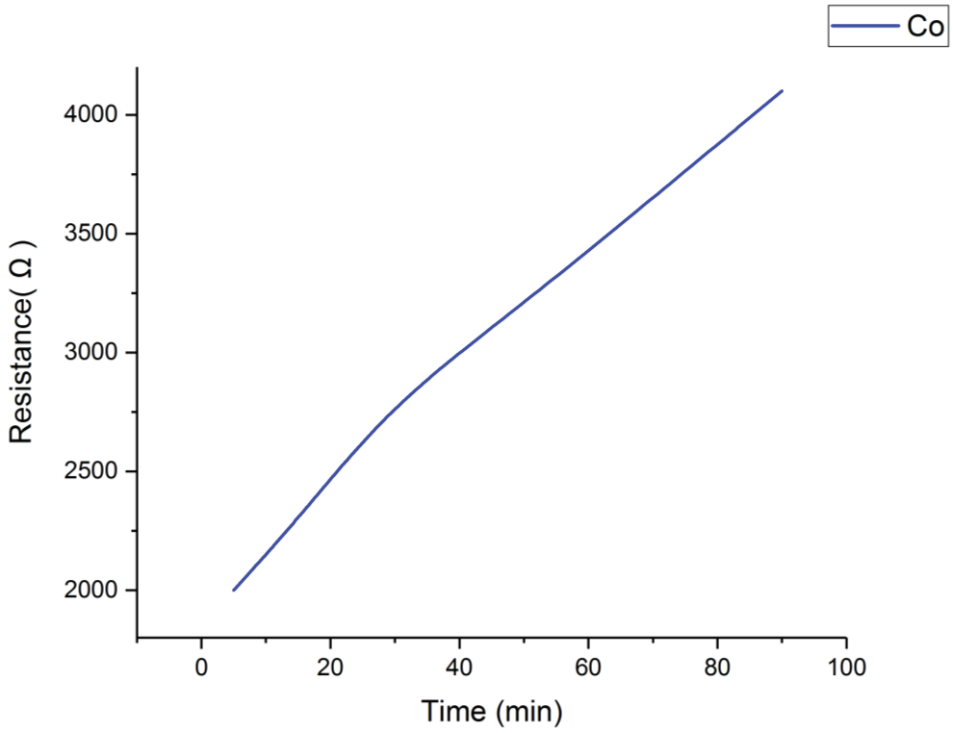

Figure 27. Bending effects on the resistance of the transparent conducting electrode fabricated by using Co catalyzed AgNWs.

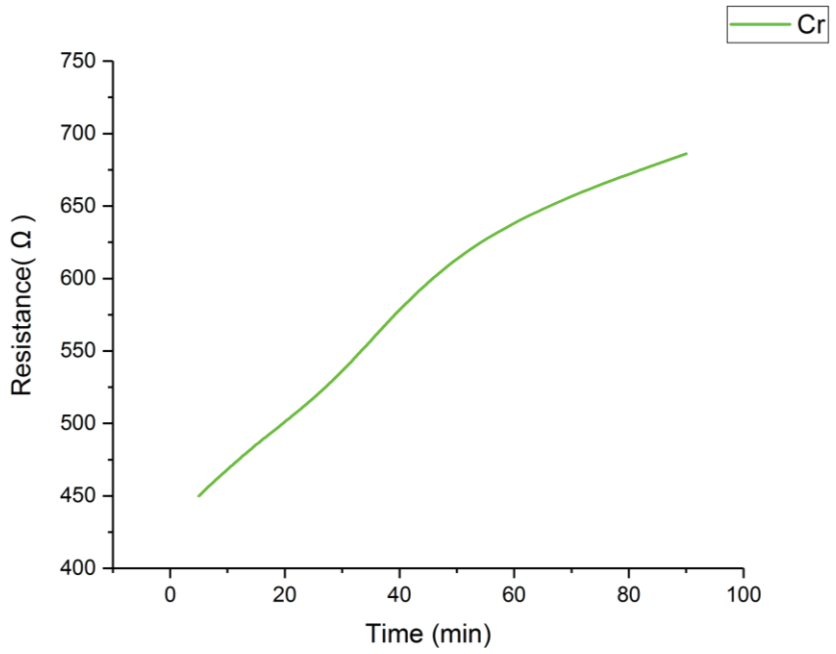

Figure 28. Bending effects on the resistance of the transparent conducting electrode fabricated by using Cr catalyzed AgNWs.

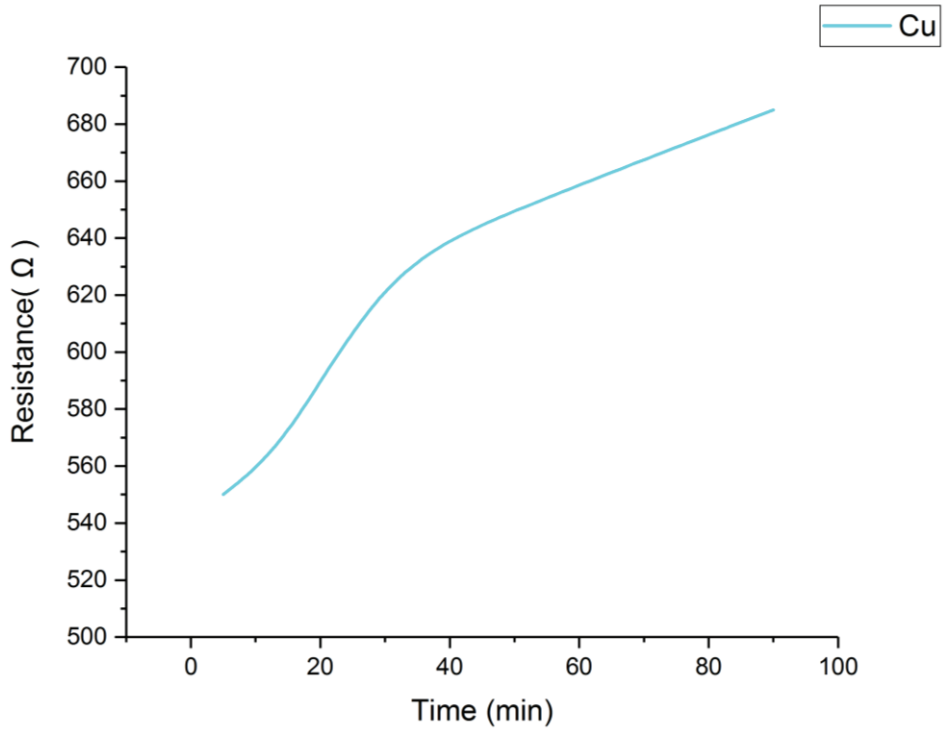

Figure 29. Bending effects on the resistance of the transparent conducting electrode fabricated by using Cu catalyzed AgNWs.

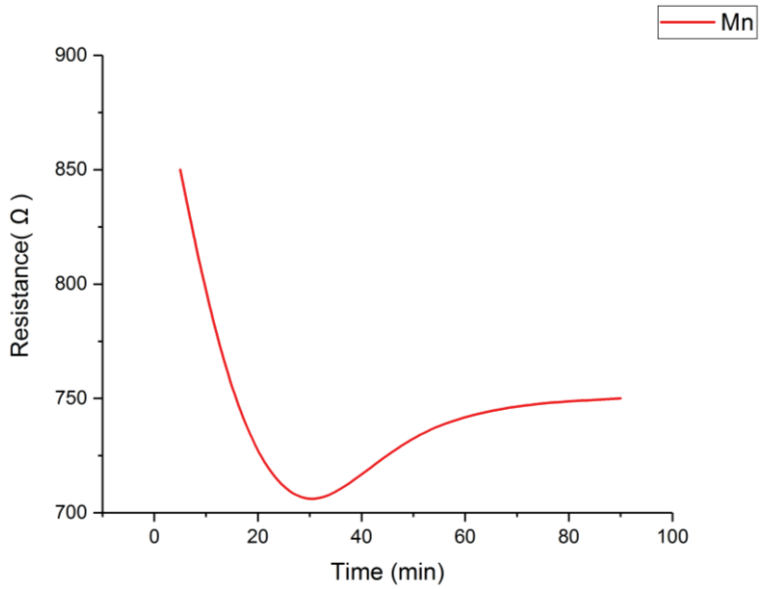

Figure 30. Bending effects on the resistance of the transparent conducting electrode fabricated by using Mn catalyzed AgNWs.

Table 2. Resistance variation of graphene-AgNWs hybrid conductive electrodes.

	Resistance (Ω)			
	Cu	Mn	Cr	Co
AgNW+Graphene	210	830	600	900
After Anneal(2h)	80	200	65	170
Flexible Form	500	1000	950	900

The Figures 23-30 show the effect of Cu, Mn, Cr, and Co catalysts used during the synthesis of AgNWs on the nanowire length and diameter, and electrical properties of the fabricated transparent conducting thin films. Table 2 summarizes the results obtained from these experiments.

CHAPTER 3

RESULTS AND DISCUSSIONS

The optical and electrical properties of the conductive electrodes are directly related to the structure of the AgNWs deposited on the solid and flexible substrates. Optical microscopy images of the AgNWs on glass substrates clearly show the length effect on the transparency of the conductive electrodes. Comparing the Cr and Mn catalyzed AgNWs, Cr catalyzed AgNWs are longer than the Mn and Co catalyzed AgNWs. This can be shown by the resistance value of the electrode before annealing; Cr electrode has 65 ohm resistance at the beginning of the annealing but the Mn electrode has 1.8 Mohm and Co electrode has 4 kohm resistances. The resistance data can be useful for the estimation of the nanowire length. However, scanning electron microscopy investigations of the AgNWs give us detailed information about the length and diameter of the nanowires. Annealing process is essential for the purification and welding of the AgNWs. Therefore, significant resistance decrease of the AgNWs has been observed by the annealing. As a result of annealing, the resistance tends to decrease to close value, even with the same type of AgNW with different transmission, Fig. 25. The polymer residues on the AgNWs were completely removed and the nanowires contact points were welded by the thermal annealing. The effect of annealing could not be observed on the transmission measurements. The 2.3% transmission decrease is observed after the graphene transfer to the conductive electrodes.(Salihoglu, Kakenov, et al. 2018) As shown in the transmittance figures, ~2.5% transmittance decrease has been observed. Owing to the interband transitions in graphene, graphene decreases transmission in the visible region of the electromagnetic spectrum about 2.3%. The difference between the theoretical and experimental data is due to the chemical residues present on the graphene coming from the graphene transfer process. Moreover, graphene transfer has dramatically improved the stability of AgNWs as a protective conductive layer. The thick layers of TMDC causes the downfall of the transmission, Fig 20 and Fig 21. Further experiments are definitely needed in order to find the optimum thickness of the TMDCs by looking at the resistance and transmission of the thin conducting film.

Flexibility test of the conductive electrode was performed by the bending process. All of the AgNWs synthesized by using different catalysts were carefully tested. The resistance value increased after bending the AgNWs but the change in resistance is negligible. There is not any considerable increase at the resistance value. Only Mn catalyzed AgNW electrode showed different characteristic at the bending test. All of these results show that AgNWs together with single layer graphene are promising candidate for next generation flexible transparent conductive electrodes. However, further experiments are definitely needed in order to fabricate graphene-AgNWs-TMDs transparent, conducting, and flexible electrodes. These electrodes can find applications in flexible electronics, solar cells, light emitting diodes, optical modulators, displays, touch and pressure sensors as well.

CHAPTER 4

CONCLUSION

After the discovery of graphene, the development of 2-dimensional materials has opened up new opportunities for applications in optoelectronic devices. Efforts to reduce the size of materials in the development of new technologies have led to the requirement for new types of electronic devices. Graphene, AgNWs, and TMDCs allowed us to increase performance of optoelectronic devices. In this thesis, flexible and transparent conductive electrodes based on AgNWs, graphene, and TMDCs have been developed and the composite structured electrode has been extensively studied. The main results achieved in this thesis can be summarized below. 1-) Large area single layer graphene was synthesized on copper foils in a CVD furnace and transferred to any rigid and flexible substrates. 2-) Silver nanowires with very small diameter and very long lengths were synthesized at high temperature in an oil bath. The mechanism of the silver nanowire formation and effects of catalysts on nanowire length and diameter have been studied extensively. 3-) Single and multi layer MoS_2 and WS_2 flakes were synthesized in a CVD furnace in an inert atmosphere. The single layer TMDCs synthesized in this work will find applications in optoelectronic device applications in future studies. 4-) Flexible and transparent conducting electrodes on rigid and flexible substrates fabricated by using single layer graphene, silver nanowires, and multilayer TMDCs. This composite structure (AgNW, graphene, and TMDC) is promising for the future applications. Further experiments are definitely required fully integrate single layer graphene with silver nanowires and a few layers TMDCs.

REFERENCES

Ataca, C., H. Şahin, and S. Ciraci. 2012. “Stable, Single-Layer MX 2 Transition-Metal Oxides and Dichalcogenides in a Honeycomb-like Structure.” *Journal of Physical Chemistry C* 116 (16): 8983–99. https://doi.org/10.1021/jp212558p.

Avouris, Phaedon. 2010. “Graphene: Electronic and Photonic Properties and Devices.” *Nano Letters* 10 (11): 4285–94. https://doi.org/10.1021/nl102824h.

Bao, Wenzhong, Jiayu Wan, Xiaogang Han, Xinghan Cai, Hongli Zhu, Dohun Kim, Dakang Ma, et al. 2014. “Approaching the Limits of Transparency and Conductivity in Graphitic Materials through Lithium Intercalation.” *Nature Communications* 5 (May): 1–9. https://doi.org/10.1038/ncomms5224.

Beams, Ryan, Luiz Gustavo Cançado, and Lukas Novotny. 2015. “Raman Characterization of Defects and Dopants in Graphene.” *Journal of Physics Condensed Matter* 27 (8). https://doi.org/10.1088/0953-8984/27/8/083002.

Berciaud, S, S Ryu, L Brus, and T Heinz. 2008. “Probing the Intrinsic Properties of Exfoliated Graphene: Raman Spectroscopy of ….” *Nano Letters*. http://arxiv.org/pdf/0901.0729%5Cnfile:///Users/keoni/Documents/Papers2/Files/Probing the Intrinsic Properties of Exfoliated Graphene Raman Spectroscopy of? - Berciaud 2008.pdf%5Cnpapers2://publication/uuid/18B1F5C3-94CE-40FC-861C-660447A3895D.

Berkelbach, Timothy C, Mark S Hybertsen, and David R Reichman. 2013. “Theory of Neutral and Charged Excitons in Monolayer Transition Metal Dichalcogenides” 045318: 1–6. https://doi.org/10.1103/PhysRevB.88.045318.

Cao, Ke, Haokun Yang, Libo Gao, Ying Han, Jingyao Feng, Hongwei Yang, Haiyan Zhang, Weidong Wang, and Yang Lu. 2020. “In Situ Mechanical Characterization of Silver Nanowire/Graphene Hybrids Films for Flexible Electronics.” *International Journal of Smart and Nano Materials*, 1–12. https://doi.org/10.1080/19475411.2020.1790056.

Castro Neto, A. H., F. Guinea, N. M.R. Peres, K. S. Novoselov, and A. K. Geim. 2009. "The Electronic Properties of Graphene." *Reviews of Modern Physics* 81 (1): 109–62. https://doi.org/10.1103/RevModPhys.81.109.

Chang, Chung Huai, Xiaofeng Fan, Shi Hsin Lin, and Jer Lai Kuo. 2013. "Orbital Analysis of Electronic Structure and Phonon Dispersion in MoS 2, MoSe2, WS2, and WSe2 Monolayers under Strain." *Physical Review B - Condensed Matter and Materials Physics* 88 (19): 1–9. https://doi.org/10.1103/PhysRevB.88.195420.

Chaves, A., J. G. Azadani, Hussain Alsalman, D. R. da Costa, R. Frisenda, A. J. Chaves, Seung Hyun Song, et al. 2020. "Bandgap Engineering of Two-Dimensional Semiconductor Materials." *Npj 2D Materials and Applications* 4 (1). https://doi.org/10.1038/s41699-020-00162-4.

Chen, Dapeng, Xueliang Qiao, Xiaolin Qiu, Jianguo Chen, and Renzhi Jiang. 2010. "Convenient Synthesis of Silver Nanowires with Adjustable Diameters via a Solvothermal Method." *Journal of Colloid and Interface Science* 344 (2): 286–91. https://doi.org/10.1016/j.jcis.2009.12.055.

Chhowalla, Manish, Hyeon Suk Shin, Goki Eda, Lain Jong Li, Kian Ping Loh, and Hua Zhang. 2013. "The Chemistry of Two-Dimensional Layered Transition Metal Dichalcogenide Nanosheets." *Nature Chemistry* 5 (4): 263–75. https://doi.org/10.1038/nchem.1589.

Chia, Xinyi, Alex Yong Sheng Eng, Adriano Ambrosi, Shu Min Tan, and Martin Pumera. 2015. "Electrochemistry of Nanostructured Layered Transition-Metal Dichalcogenides." *Chemical Reviews* 115 (21): 11941–66. https://doi.org/10.1021/acs.chemrev.5b00287.

Choi, Wonbong, Indranil Lahiri, Raghunandan Seelaboyina, and Yong Soo Kang. 2010. "Synthesis of Graphene and Its Applications: A Review." *Critical Reviews in Solid State and Materials Sciences* 35 (1): 52–71. https://doi.org/10.1080/10408430903505036.

Conley, Hiram J., Bin Wang, Jed I. Ziegler, Richard F. Haglund, Sokrates T. Pantelides, and Kirill I. Bolotin. 2013. "Bandgap Engineering of Strained Monolayer and Bilayer MoS2." *Nano Letters* 13 (8): 3626–30. https://doi.org/10.1021/nl4014748.

Das, Anindya, Biswanath Chakraborty, and A. K. Sood. 2008. “Raman Spectroscopy of Graphene on Different Substrates and Influence of Defects.” *Bulletin of Materials Science* 31 (3): 579–84. https://doi.org/10.1007/s12034-008-0090-5.

Datar, Avdhoot, Maya Bar-Sadan, and Ashwin Ramasubramaniam. 2020. “Interactions between Transition-Metal Surfaces and MoS2Monolayers: Implications for Hydrogen Evolution and CO2Reduction Reactions.” *Journal of Physical Chemistry C* 124 (37): 20116–24. https://doi.org/10.1021/acs.jpcc.0c05191.

Dresselhaus, M. S., A. Jorio, A. G. Souza Filho, and R. Saito. 2010. “Defect Characterization in Graphene and Carbon Nanotubes Using Raman Spectroscopy.” *Philosophical Transactions of the Royal Society A: Mathematical, Physical and Engineering Sciences* 368 (1932): 5355–77. https://doi.org/10.1098/rsta.2010.0213.

Ferrari, Andrea C. 2007. “Raman Spectroscopy of Graphene and Graphite: Disorder, Electron-Phonon Coupling, Doping and Nonadiabatic Effects.” *Solid State Communications* 143 (1–2): 47–57. https://doi.org/10.1016/j.ssc.2007.03.052.

Gan, Sheng, Yupeng Zhang, and Qiaoliang Bao. 2017. “Graphene-Based Optical Modulators.” *Graphene Photonics, Optoelectronics, and Plasmonics*, no. March: 41–56. https://doi.org/10.1201/9781315196671.

Ganorkar, Shraddha, Jungyoon Kim, Young Hwan Kim, and Seong-il Kim. n.d. “Effect of Precursor on Growth of MoS 2 Monolayer and Multilayer,” 1–4.

Gao, Yang, Zhibo Liu, Dong Ming Sun, Le Huang, Lai Peng Ma, Li Chang Yin, Teng Ma, et al. 2015. “Large-Area Synthesis of High-Quality and Uniform Monolayer WS2 on Reusable Au Foils.” *Nature Communications* 6: 1–10. https://doi.org/10.1038/ncomms9569.

Hu, Liangbing, Han Sun Kim, Jung Yong Lee, Peter Peumans, and Yi Cui. 2010. “Scalable Coating and Properties of Transparent, Flexible, Silver Nanowire Electrodes.” *ACS Nano* 4 (5): 2955–63. https://doi.org/10.1021/nn1005232.

Huang, Xiao, Zongyou Yin, Shixin Wu, Xiaoying Qi, Qiyuan He, Qichun Zhang, Qingyu Yan, Freddy Boey, and Hua Zhang. 2011. "Graphene-Based Materials: Synthesis, Characterization, Properties, and Applications." *Small* 7 (14): 1876–1902. https://doi.org/10.1002/smll.201002009.

Jariwala, Deep, Tobin J. Marks, and Mark C. Hersam. 2017. "Mixed-Dimensional van Der Waals Heterostructures." *Nature Materials* 16 (2): 170–81. https://doi.org/10.1038/nmat4703.

Jia, Changchao, Ping Yang, and Aiyu Zhang. 2014. "Glycerol and Ethylene Glycol Co-Mediated Synthesis of Uniform Multiple Crystalline Silver Nanowires." *Materials Chemistry and Physics* 143 (2): 794–800. https://doi.org/10.1016/j.matchemphys.2013.10.015.

Jin, Yunxia, Yong Sun, Kaiqing Wang, Yani Chen, Ziqi Liang, Yuxi Xu, and Fei Xiao. 2018. "Long-Term Stable Silver Nanowire Transparent Composite as Bottom Electrode for Perovskite Solar Cells." *Nano Research* 11 (4): 1998–2011. https://doi.org/10.1007/s12274-017-1816-8.

Jo, Yong Jin, Chaewon Kim, Jun Hyeok Lee, Mu Seok Ko, Anjae Jo, Jin Yeol Kim, Woo Gwang Jung, et al. 2016. "Development of Patterned 1D Metal Nanowires with Adhesion Layer for Mesh Electrodes of Flexible Transparent Conductive Films for Touch Screen Panels." *Journal of Nanoscience and Nanotechnology* 16 (11): 11586–90. https://doi.org/10.1166/jnn.2016.13556.

K. S. Novoselov, A. K. Geim, S. V. Morozov, D. Jiang, Y. Zhang, S. V. Dubonos, I. V. Grigorieva and A. A. Firsov. 2016. "Electric Field Effect in Atomically Thin Carbon Films" 306 (5696): 666–69.

Kahl, Günter. 2015. "T Ip- e Nhanced R Aman s Pectroscopy (TERS) ." *The Dictionary of Genomics, Transcriptomics and Proteomics*, 1–1. https://doi.org/10.1002/9783527678679.dg13293.

Kang, Kyung Nam, Kyle Godin, and Eui Hyeok Yang. 2015. "The Growth Scale and Kinetics of WS2 Monolayers under Varying H2 Concentration." *Scientific Reports* 5: 1–10. https://doi.org/10.1038/srep13205.

Khairuzzaman, M Qadafi. 2016. “No Title血清及尿液特定蛋白检测在糖尿病肾病早期诊断中的意义” 4 (1): 64–75.

Kim, Byoung Soo, Jun Beom Pyo, Jeong Gon Son, Goangseup Zi, Sang Soo Lee, Jong Hyuk Park, and Jonghwi Lee. 2017. “Biaxial Stretchability and Transparency of Ag Nanowire 2D Mass-Spring Networks Prepared by Floating Compression.” *ACS Applied Materials and Interfaces* 9 (12): 10865–73. https://doi.org/10.1021/acsami.7b00449.

Kim, Myungwoong, Nathaniel S. Safron, Changshui Huang, Michael S. Arnold, and Padma Gopalan. 2012. “Light-Driven Reversible Modulation of Doping in Graphene.” *Nano Letters* 12 (1): 182–87. https://doi.org/10.1021/nl2032734.

Kuc, Agnieszka, and Thomas Heine. 2015. “The Electronic Structure Calculations of Two-Dimensional Transition-Metal Dichalcogenides in the Presence of External Electric and Magnetic Fields.” *Chemical Society Reviews* 44 (9): 2603–14. https://doi.org/10.1039/c4cs00276h.

Lagrange, M., D. P. Langley, G. Giusti, C. Jiménez, Y. Bréchet, and D. Bellet. 2015. “Optimization of Silver Nanowire-Based Transparent Electrodes: Effects of Density, Size and Thermal Annealing.” *Nanoscale* 7 (41): 17410–23. https://doi.org/10.1039/c5nr04084a.

Lan, Feifei, Ruixia Yang, Yongkuan Xu, Shengya Qian, Song Zhang, Hongjuan Cheng, and Ying Zhang. 2018. “Synthesis of Large-Scale Single-Crystalline Monolayer WS2 Using a Semi-Sealed Method.” *Nanomaterials* 8 (2): 1–8. https://doi.org/10.3390/nano8020100.

Langley, Daniel, Gaël Giusti, Céline Mayousse, Caroline Celle, Daniel Bellet, and Jean Pierre Simonato. 2013. “Flexible Transparent Conductive Materials Based on Silver Nanowire Networks: A Review.” *Nanotechnology* 24 (45). https://doi.org/10.1088/0957-4484/24/45/452001.

Lee, Changgu, Hugen Yan, Louis E. Brus, Tony F. Heinz, James Hone, and Sunmin Ryu. 2010. “Anomalous Lattice Vibrations of Single- and Few-Layer MoS2.” *ACS Nano* 4 (5): 2695–2700. https://doi.org/10.1021/nn1003937.

Lee, Eduardo J.H., Kannan Balasubramanian, Ralf Thomas Weitz, Marko Burghard, and Klaus Kern. 2008. "Contact and Edge Effects in Graphene Devices." *Nature Nanotechnology* 3 (8): 486–90. https://doi.org/10.1038/nnano.2008.172.

Li, Dongdong, Wen Yong Lai, Yi Zhou Zhang, and Wei Huang. 2018. "Printable Transparent Conductive Films for Flexible Electronics." *Advanced Materials* 30 (10): 1–24. https://doi.org/10.1002/adma.201704738.

Li, Yuxiu, Ximin Yuan, Hongwei Yang, Yunxiu Chao, Shuailong Guo, and Chuan Wang. 2019. "One-Step Synthesis of Silver Nanowires with Ultra-Long Length and Thin Diameter to Make Flexible Transparent Conductive Films." *Materials* 12 (3). https://doi.org/10.3390/ma12030401.

Li, Z. Q., E. A. Henriksen, Z. Jiang, Z. Hao, M. C. Martin, P. Kim, H. L. Stormer, and D. N. Basov. 2008. "Dirac Charge Dynamics in Graphene by Infrared Spectroscopy." *Nature Physics* 4 (7): 532–35. https://doi.org/10.1038/nphys989.

Liu, Leitao, S. Bala Kumar, Yijian Ouyang, and Jing Guo. 2011. "Performance Limits of Monolayer Transition Metal Dichalcogenide Transistors." *IEEE Transactions on Electron Devices* 58 (9): 3042–47. https://doi.org/10.1109/TED.2011.2159221.

Liu, Yuan, Nathan O. Weiss, Xidong Duan, Hung Chieh Cheng, Yu Huang, and Xiangfeng Duan. 2016. "Van Der Waals Heterostructures and Devices." *Nature Reviews Materials* 1 (9). https://doi.org/10.1038/natrevmats.2016.42.

Mahmoodi, Nosrat O., Atefeh Ghavidast, Mitra Ashkan, Manouchehr Mamaghani, Mohammad Ali Zanjanchi, Khalil Tabatabaeian, and Armin Arabanian. 2016. "Efficient Synthesis of (S)-(+)-Clopidogrel Bisulfate-Capped Silver Nanoparticles." *Synthesis and Reactivity in Inorganic, Metal-Organic and Nano-Metal Chemistry* 46 (10): 1552–57. https://doi.org/10.1080/15533174.2015.1137028.

Mak, Kin Fai, Changgu Lee, James Hone, Jie Shan, and Tony F. Heinz. 2010. "Atomically Thin MoS2: A New Direct-Gap Semiconductor." *Physical Review Letters* 105 (13): 2–5. https://doi.org/10.1103/PhysRevLett.105.136805.

Malard, L. M., M. A. Pimenta, G. Dresselhaus, and M. S. Dresselhaus. 2009. “Raman Spectroscopy in Graphene.” *Physics Reports* 473 (5–6): 51–87. https://doi.org/10.1016/j.physrep.2009.02.003.

Meng, Lili, Ruixin Bian, Cheng Guo, Bojie Xu, Huan Liu, and Lei Jiang. 2018. “Aligning Ag Nanowires by a Facile Bioinspired Directional Liquid Transfer: Toward Anisotropic Flexible Conductive Electrodes.” *Advanced Materials* 30 (25): 1–9. https://doi.org/10.1002/adma.201706938.

Morichi, Shigeaki, Yukinori Okahiro, Yooichi Komoda, Hirohisa Inagaki, and Hiroyuki Itami. 2008. “Examination on the Vertical Normal Strain Observed at the Grounds Surface during Earthquakes.” *Doboku Gakkai Ronbunshuu A* 64 (2): 452–57. https://doi.org/10.2208/jsceja.64.452.

Mutiso, Rose M, Michelle C Sherrott, Aaron R Rathmell, Benjamin J Wiley, Karen I Winey, Materials Science, United States, North Carolina, and United States. 2013. “Rose M. Mutiso, † Michelle C. Sherrott, † Aaron R. Rathmell, ‡ Benjamin J. Wiley, ‡ and Karen I. Winey †, * Department of Materials Science and Engineering, University of Pennsylvania, Philadelphia, Pennsylvania 19104, United States, and ‡ Department of C,” no. 9: 7654–63.

Nair, R. R., P. Blake, A. N. Grigorenko, K. S. Novoselov, T. J. Booth, T. Stauber, N. M.R. Peres, and A. K. Geim. 2008. “Fine Structure Constant Defines Visual Transparency of Graphene.” *Science* 320 (5881): 1308. https://doi.org/10.1126/science.1156965.

Ni, Zhenhua, Yingying Wang, Ting Yu, and Zexiang Shen. 2008. “Raman Spectroscopy and Imaging of Graphene.” *Nano Research* 1 (4): 273–91. https://doi.org/10.1007/s12274-008-8036-1.

Novoselov, K. S., A. Mishchenko, A. Carvalho, and A. H. Castro Neto. 2016. “2D Materials and van Der Waals Heterostructures.” *Science* 353 (6298). https://doi.org/10.1126/science.aac9439.

Partoens, B., and F. M. Peeters. 2006. “From Graphene to Graphite: Electronic Structure around the K Point.” *Physical Review B - Condensed Matter and Materials Physics* 74 (7): 1–11. https://doi.org/10.1103/PhysRevB.74.075404.

Plechinger, G., S. Heydrich, M. Hirmer, F.-X. Schrettenbrunner, D. Weiss, J. Eroms, C. Schüller, and T. Korn. 2012. " Scanning Raman Spectroscopy of Few- and Single-Layer MoS 2 Flakes ." *Nanoengineering: Fabrication, Properties, Optics, and Devices IX* 8463 (0): 84630N. https://doi.org/10.1117/12.928068.

Qiao, Shuai, Hang Yang, Zongqi Bai, Gang Peng, and Xueao Zhang. 2017. "Identifying the Number of WS2 Layers via Raman and Photoluminescence Spectrum" 141 (Icmmcce): 1408–13. https://doi.org/10.2991/icmmcce-17.2017.247.

Ross, Jason S., Sanfeng Wu, Hongyi Yu, Nirmal J. Ghimire, Aaron M. Jones, Grant Aivazian, Jiaqiang Yan, et al. 2013. "Electrical Control of Neutral and Charged Excitons in a Monolayer Semiconductor." *Nature Communications* 4: 1473–76. https://doi.org/10.1038/ncomms2498.

Saito, R., M. Hofmann, G. Dresselhaus, A. Jorio, and M. S. Dresselhaus. 2011. "Raman Spectroscopy of Graphene and Carbon Nanotubes." *Advances in Physics* 60 (3): 413–550. https://doi.org/10.1080/00018732.2011.582251.

Salihoglu, Omer, Nurbek Kakenov, Osman Balci, Sinan Balci, and Coskun Kocabas. 2016. "Graphene as a Reversible and Spectrally Selective Fluorescence Quencher." *Scientific Reports* 6 (September): 1–7. https://doi.org/10.1038/srep33911.

Salihoglu, O., Kakenov, N., Balci, O., Balci, S., & Kocabas, C. (2018). Graphene-Quantum dot Hybrid Optoelectronics at visible wavelengths. ACS Photonics, 5(6), 2384-2390. doi:10.1021/acsphotonics.8b00163.

Salihoglu, Omer, Hasan Burkay Uzlu, Ozan Yakar, Shahnaz Aas, Osman Balci, Nurbek Kakevov, Sinan Balci, Selim Olcum, Sefik Süzer, and Coskun Kocabas. 2018. "Graphene Based Adaptive Thermal Camouflage." *ArXiv*, 1–21.

Senthilkumar, V., Le C. Tam, Yong Soo Kim, Yumin Sim, Maeng Je Seong, and Joon I. Jang. 2014. "Direct Vapor Phase Growth Process and Robust Photoluminescence Properties of Large Area MoS2 Layers." *Nano Research* 7 (12): 1759–68. https://doi.org/10.1007/s12274-014-0535-7.

Solomon, Edward I. 1980. *Spectroscopic Properties of Inorganic and Organometallic Compounds*. *Journal of Organometallic Chemistry*. Vol. 192. https://doi.org/10.1016/s0022-328x(00)93346-1.

Splendiani, Andrea, Liang Sun, Yuanbo Zhang, Tianshu Li, Jonghwan Kim, Chi Yung Chim, Giulia Galli, and Feng Wang. 2010. "Emerging Photoluminescence in Monolayer MoS2." *Nano Letters* 10 (4): 1271–75. https://doi.org/10.1021/nl903868w.

Sun, Zhipei, Tawfique Hasan, Felice Torrisi, Daniel Popa, Giulia Privitera, Fengqiu Wang, Francesco Bonaccorso, Denis M. Basko, and Andrea C. Ferrari. 2010. "Graphene Mode-Locked Ultrafast Laser." *ACS Nano* 4 (2): 803–10. https://doi.org/10.1021/nn901703e.

Tang, Bo, Hu Guoxin, and Hanyang Gao. 2010. "Raman Spectroscopic Characterization of Graphene." *Applied Spectroscopy Reviews* 45 (5): 369–407. https://doi.org/10.1080/05704928.2010.483886.

Toh, Rou Jun, Zdeněk Sofer, Jan Luxa, David Sedmidubský, and Martin Pumera. 2017. "3R Phase of MoS2 and WS2 Outperforms the Corresponding 2H Phase for Hydrogen Evolution." *Chemical Communications* 53 (21): 3054–57. https://doi.org/10.1039/c6cc09952a.

Trung, Tran Nam, Vinaya Kumar Arepalli, Rajesh Gudala, and Eui Tae Kim. 2017. "Polyol Synthesis of Ultrathin and High-Aspect-Ratio Ag Nanowires for Transparent Conductive Films." *Materials Letters* 194: 66–69. https://doi.org/10.1016/j.matlet.2017.02.011.

Tseng, Sian Hong, Lian Ming Lyu, Kai Yuan Hsiao, Wan Hua Ho, and Ming Yen Lu. 2020. "Surfactant-Free Synthesis of Ultralong Silver Nanowires for Durable Transparent Conducting Electrodes." *Chemical Communications* 56 (42): 5593–96. https://doi.org/10.1039/d0cc01915a.

Wang, Hai I., Marie Luise Braatz, Nils Richter, Klaas Jan Tielrooij, Zoltan Mics, Hao Lu, Nils Eike Weber, et al. 2017. "Reversible Photochemical Control of Doping Levels in Supported Graphene." *Journal of Physical Chemistry C* 121 (7): 4083–91. https://doi.org/10.1021/acs.jpcc.7b00347.

Wang, Jingang, Fengcai Ma, Wenjie Liang, and Mengtao Sun. 2017. “Electrical Properties and Applications of Graphene, Hexagonal Boron Nitride (h-BN), and Graphene/h-BN Heterostructures.” *Materials Today Physics* 2: 6–34. https://doi.org/10.1016/j.mtphys.2017.07.001.

Wang, Qing Hua, Kourosh Kalantar-Zadeh, Andras Kis, Jonathan N. Coleman, and Michael S. Strano. 2012. “Electronics and Optoelectronics of Two-Dimensional Transition Metal Dichalcogenides.” *Nature Nanotechnology* 7 (11): 699–712. https://doi.org/10.1038/nnano.2012.193.

Weng, Qunhong, Guodong Li, Xinliang Feng, Kornelius Nielsch, Dmitri Golberg, and Oliver G. Schmidt. 2018. “Electronic and Optical Properties of 2D Materials Constructed from Light Atoms.” *Advanced Materials* 30 (46). https://doi.org/10.1002/adma.201801600.

Wu, Jiang Bin, Miao Ling Lin, Xin Cong, He Nan Liu, and Ping Heng Tan. 2018. “Raman Spectroscopy of Graphene-Based Materials and Its Applications in Related Devices.” *Chemical Society Reviews* 47 (5): 1822–73. https://doi.org/10.1039/c6cs00915h.

Yakar, Ozan. 2020. “INVESTIGATION OF PHOTODETECTORS USING GRAPHENE FIELD EFFECT TRANSISTORS IN COMBINATION WITH FUNCTIONAL DYE MATERIALS A Thesis Submitted To,” no. July.

Yan, Jun, Yuanbo Zhang, Philip Kim, and Aron Pinczuk. 2007. “Electric Field Effect Tuning of Electron-Phonon Coupling in Graphene.” *Physical Review Letters* 98 (16): 1–4. https://doi.org/10.1103/PhysRevLett.98.166802.

Zhang, Dongbai, Limin Qi, Jinhu Yang, Jiming Ma, Humin Cheng, and Lan Huang. 2004. “Wet Chemical Synthesis of Silver Nanowire Thin Films at Ambient Temperature.” *Chemistry of Materials* 16 (5): 872–76. https://doi.org/10.1021/cm0350737.

Zhang, Fu, Yanfu Lu, Daniel S. Schulman, Tianyi Zhang, Kazunori Fujisawa, Zhong Lin, Yu Lei, et al. 2019. “Carbon Doping of WS2 Monolayers: Bandgap Reduction and p-Type Doping Transport.” *Science Advances* 5 (5). https://doi.org/10.1126/sciadv.aav5003.

Zhao, Kai, Qifei Chang, Xing Chen, Buchang Zhang, and Jinhuai Liu. 2009. “Synthesis and Application of DNA-Templated Silver Nanowires for Ammonia Gas Sensing.” *Materials Science and Engineering C* 29 (4): 1191–95. https://doi.org/10.1016/j.msec.2008.09.045.

Zhu, Yanwu, Shanthi Murali, Weiwei Cai, Xuesong Li, Ji Won Suk, Jeffrey R. Potts, and Rodney S. Ruoff. 2010. “Graphene and Graphene Oxide: Synthesis, Properties, and Applications.” *Advanced Materials* 22 (35): 3906–24. https://doi.org/10.1002/adma.201001068.